The CDC42-interacting protein 4 controls epithelial cell cohesion and tumor dissemination

The CDC42-interacting protein 4 controls epithelial cell-cohesion and tumor dissemination

Yannève Rolland[1,*], Paola Marighetti[1,*], Chiara Malinverno[1], Stefano Confalonieri[1,2], Chiara Luise[1,2], Nadia Ducano[3], Andrea Palamidessi[1], Sara Bisi[1], Hiroaki Kajiho[1], Flavia Troglio[1,2], Olga G.Shcherbakova[5], Alexander R. Dunn[5], Amanda Oldani[1], Letizia Lanzetti[3], Pier Paolo Di Fiore[1,2,4], Andrea Disanza, and Giorgio Scita[1,4]

[1]IFOM, Fondazione Istituto FIRC di Oncologia Molecolare, Via Adamello 16, 20139 Milano, Italy;
[2]Dipartimento di Oncologia Sperimentale, Istituto Europeo di Oncologia, 20141 Milano, Italy;
[3]Dipartimento di Scienze Oncologiche, Università degli Studi di Torino, Istituto per la Ricerca e la Cura del Cancro, Str. Provinciale 142 10060 Candiolo, Torino, Italy;
[4]Dipartimento di Scienze della Salute, San Paolo, Università degli Studi di Milano, 20122 Milan, Italy.
[5]Departments of Chemical Engineering,Stanford University, Stanford, CA 94305

[*]These authors equally contributed to the work

Correspondence should be addressed to:

Giorgio Scita
IFOM Foundation, Institute FIRC of Molecular Oncology
Via Adamello, 16
20139, Milano
Tel: +39-02-574303277
FAX: +39-02-574303231
e-mail: giorgio.scita@ifom.eu
or
andrea.disanza@ifom.eu

Running Title:

CIP4 controls cell cohesion and tumor invasion

Summary

The role of endocytic proteins and the molecular mechanisms underlying epithelial cell cohesion and tumor dissemination are not well understood. Here, we report that the endocytic F-BAR-containing CDC42-interacting protein 4 (CIP4) is upregulated in ERBB2-positive human breast cancer (BC), correlates with increased distant metastasis, and is an independent predictor of poor disease outcome in subsets of BC patients. Consistently, CIP4 is required for ERBB2- and TGF-ß1-induced cell scattering, motility and invasion into 3D matrices by BC lines and for the conversion from ductal breast carcinoma *in situ* to invasive carcinoma in mouse xenograft models. In normal and tumorigenic derivatives of MCF10A breast epithelial cells, depletion of CIP4 induces cell compaction and impairs EGF-induced cell scattering, motility and invasion. These defects are not due to altered EGFR signaling or trafficking, but to impaired EGF-induced E-cadherin endocytosis and actomyosin contractility, which is required to generate tangential forces to break cell-cell junctions. At the molecular level, CIP4 promotes the formation of an E-cadherin-CIP4-SRC complex that controls SRC activation, E-cadherin endocytosis and localized phosphorylation of the myosin light chain kinase. Thus, CIP4 critically controls cell-cell cohesion and is required for the acquisition of an invasive phenotype in breast tumors.

Introduction

Epithelial cells organize into polarized, coherent sheets of cells, whose architecture is dependent on the formation of cell-cell adhesion structures. A key component of epithelial junctions in vertebrates is the transmembrane protein E-cadherin, which defines the so-called adherens junction (AJ) (Reynolds and Roczniak-Ferguson, 2004; Zhurinsky et al., 2000). AJs undergo rapid assembly and disassembly to enable epithelial tissue morphogenesis and rearrangement, as well as the acquisition of cell motility during epithelial-mesenchymal transition (EMT) (Thiery et al., 2009). However, how cell-cell adhesion is disrupted during EMT is poorly understood. The key event in this process is the loss of E-cadherin-mediated cell-cell adhesion, mostly likely as a consequence of reduced E-cadherin transcription, although alternative mechanisms might exist.

A wealth of recent evidence points to a crucial role of E-cadherin endocytosis and recycling in tissue morphogenesis and EMT (Blankenship et al., 2007; Bryant and Stow, 2004; Langevin et al., 2005; Paterson et al., 2003; Shaye et al., 2008). Endocytic removal of E-cadherin from the cell surface is frequently and acutely induced by activation of receptor (Orlichenko et al., 2009) and non-receptor (Avizienyte et al., 2002) tyrosine kinases, as well as by stimulation with transforming growth factor-β (TGF-β) (Janda et al., 2006). In the case of epidermal growth factor (EGF)-induced E-cadherin downregulation and AJ disassembly, SRC has an important role. SRC forms complexes with E-cadherin and the EGF receptor (EGFR) (Shen et al., 2008), and, upon activation, promotes EMT by phosphorylating E-cadherin and triggering its ubiquitination-dependent endocytosis and degradation (Behrens, 1999; Fujita et al., 2002b). Cell-cell adhesion can, in turn, modulate growth factor signaling (Qian et al., 2004; Reshetnikova et al., 2007), suggesting that E-cadherin endocytosis and signal transduction from receptor tyrosine kinases (RTKs) are intimately intertwined in the maintenance of epithelial cell morphogenesis, as well as in controlling epithelial cell motility. Our understanding of the molecular circuitry involved in this crosstalk, however, is still incomplete. It is unclear how RTK activation induces E-cadherin dynamics and trafficking, what the key molecular determinants underlying this process are, and how E-cadherin endocytic machinery affects junctional tension.

One set of proteins that is ideally positioned to control E-cadherin trafficking and junctional stability is the FCH-Bin-Amphiphysin-Rvs (F-BAR)-domain containing proteins. In mammals, F-BAR proteins (hereafter referred to as the TOCA family) include three members: TOCA-1 (Transducer of CDC42-dependent actin assembly), CIP4 (CDC42-interacting protein 4) and FBP17 (formin-binding protein 17). These proteins are implicated in clathrin-mediated endocytosis (CME), during which they sense and promote membrane curvature through their F-BAR domain, and bind to key actin dynamics (e.g., the nucleation promoting factor N-WASP) and endocytic (e.g.,

dynamin) regulators through their SH3 domain (Ho et al., 2004; Itoh et al., 2005; Tian et al., 2000). Furthermore, TOCA-1 and CIP4, through their HR1/CRIB (Homology Region1/CDC42 and Rac interacting binding motif)-like domain, act as effectors of the small GTPase CDC42 (Aspenstrom, 1997; Ho et al., 2004; Itoh et al., 2005; Tian et al., 2000). We have recently shown that in *C. elegans*, TOCA family proteins localize at cell-cell junctions, where they regulate the organization of cortical F-actin and the levels of the junctional protein AJM-1(Giuliani et al., 2009). Similarly, the single *Drosophila* TOCA protein, dCIP4, contributes to E-cadherin trafficking by connecting the CDC42-dependent polarity complex, PAR-6/aPKC, with WASP and dynamin, ultimately regulating vesicle scission and internalization of E-cadherin (Balklava et al., 2007; Georgiou et al., 2008; Harris and Tepass, 2008; Leibfried et al., 2008). However, the functional role of this protein family in mammalian epithelial cell morphogenesis and epithelial tumor cell dissemination is unknown.

Here, using a systematic RNAi approach to silence TOCA family proteins in normal and tumorigenic mammary epithelial cells, we show that CIP4, by regulating E-cadherin internalization and junctional actomyosin contractility, controls cell scattering, EMT and invasion in response to various motogenic signals. We further show that CIP4 elevated expression is selected in ERBB2+ and triple negative breast cancer tumors and correlates with increased risk of distant metastasis. Consistently, CIP4 is required for the conversion from ductal carcinoma *in situ* (DCIS) to invasive ductal carcinoma (IDC) in mouse xenograft models.

Results

CIP4 controls MCF10A cell cohesion

To investigate the hypothesis that the TOCA family proteins are involved in epithelial morphogenesis also in mammals, we silenced each of the members of the family in normal human mammary epithelial cells MCF10A, either individually (CIP4-knockdown [KD] #1 and #2 obtained using two different lentiviruses; TOCA1-KD; FBP17-KD) or in combination (CIP4/TOCA-1 or CIP4/FBP17 double knockdown [2KD]; CIP4/TOCA-1/FBP17 triple knockdown [3KD]) (Fig. 1A). Phase contrast microscopy revealed that CIP4-depleted cells, but not scramble-control, TOCA1-KD or FBP17-KD cells, tended to cluster into cohesive colonies despite the presence of EGF in the medium, which is required for MCF10A growth and normally induces a scattered cell phenotype (Debnath et al., 2003; Singh et al., 2009) (Fig. 1B). We quantified these morphological phenotypes and confirmed that removal of CIP4 significantly increased the number of tightly compacted colonies and concomitantly reduced the number of single isolated cells (Fig. 1C). Notably, the simultaneous silencing of two or all three TOCA family proteins did not augment the proportion of compact colonies *vs.* single cells observed following depletion of CIP4 alone (Fig. 1C and Fig. S1A). In line with these data, reconstitution of CIP4 in CIP4-KD cells, using an RNAi-resistant GFP-CIP4 expressed at levels comparable to the endogenous protein, restored a scattered cell phenotype, with significantly fewer and less compact cell clusters than in CIP4-KD cultures (Fig. 1D-F). Thus, removal of CIP4, but not of other TOCA family members, enhances cell cohesion and the formation of tightly adherent cell clusters.

We next characterized the main structural and molecular features of the compact cell clusters. We investigated the status of cell-cell junctions after removal of CIP4, focusing on AJs. E-cadherin displayed the expected localization at cell-cell contacts and in intracellular vesicular structures in all lines tested (Fig. S1B-C). However, CIP4-depletion caused a marked increase in junctional E-cadherin in clustered cells (Fig. S1B-C). Although E-cadherin participates in the regulation of cell growth by mediating homophilic cell-cell adhesion and contact inhibition of growth (Gumbiner, 2005), the increased levels of junctional E-cadherin in CIP4-depleted cells did not influence their rate of cell proliferation (Fig. S1D). The formation of compact colonies following CIP4 removal was also accompanied by a homogenous distribution of the Golgi complex that was oriented in the majority of clustered CIP4-KD cells (>70%) towards the free-facing surface of the cell (Fig. S2E). In contrast, control cells formed loosely adherent colonies, which displayed a randomly oriented Golgi complex, even in cells engaged in junctional contacts along three sides (compare insets in Fig. S1E). Additionally, CIP4-KD cell colonies displayed thick F-actin cables extending along the external cortex, while F-actin was reduced along cell-cell junctions as

compared to scramble-control or TOCA-1-KD and FBP17-KD cells (Fig. S1F). Collectively, these findings indicate that CIP4 is unique among the TOCA family members in that it regulates cell cohesion and junctional adhesion of MCF10A cells.

CIP4 does not influence motility parameters of individual MCF10A cells, but indirectly controls the motility behavior

The dynamic remodeling of cell-cell junctions is crucial for epithelial tissue plasticity and cell motility. Thus, we tested, by time-lapse microscopy, the motility of the different MCF10A TOCA family-KD cells. In the presence of EGF, control cells were scattered and highly motile, frequently coming into contact with each other and moving apart soon after. In contrast, CIP4-KD cells tended to aggregate into clusters and ceased migration (Movie S1). Indeed, quantification of motility parameters indicated that CIP4-KD cells displayed markedly reduced velocity once they encountered a cell cluster (Fig. S2A). However, isolated CIP4-KD cells moved at a similar speed to control cells (Fig. S2B), arguing that CIP4 has no major effect on the basic cell locomotion machinery. Similar migratory parameters and behavior were observed in the 2KD and 3KD cells (Fig. S2A-B), whereas, TOCA1-KD and FBP17-KD MCF10A cells resembled control cells, albeit removal of FBP17 reduced slightly, but not significantly, cell velocity (Fig. S2A-B and Movies S1). Thus, removal of CIP4 alone is responsible for the aberrant migratory phenotype. Notably, all cell lines eventually formed an epithelial monolayer and established stable cell-cell junctions. Additionally, the ability of MCF10A cells to migrate into a wound as a cohesive cohort was not affected by removal of CIP4 (Fig. S2C) or of other TOCA family members (data not shown). Together, these results suggest that CIP4 indirectly controls motility behavior, likely by stabilizing AJs, even under conditions in which junctional dynamics is enhanced by the activation of EGFR signaling.

CIP4 is required for EGF-induced scattering of MCF10A cells, but does not affect EGFR signaling, trafficking and CDC42-N-WASP activation

MCF10A cells require EGF to maintain epithelial features (Petersen et al., 1992). In the presence of EGF, control MCF10A cells typically scattered over the available space and failed to form stable cell-cell contacts (Fig. S2D). Conversely, after EGF deprivation, control cells, as well as TOCA1-KD and FBP17-KD cells, aggregated forming compact cell clusters, with a prominent cortical actin ring and junction-restricted E-cadherin, reminiscent of the phenotypic behavior of CIP4-KD cells grown in the presence of EGF (Fig. S2D-E). These results suggest that CIP4-KD cells might be defective in responding to acute EGF stimulation. To test this possibility, we performed EGF-induced cell scattering assays. Control and CIP4-KD cells deprived of EGF form

compact clusters. Within a few minutes of EGF stimulation, control cells became very motile, extending elongated cell protrusions away from the cluster, and were almost completely scattered 2 h after EGF addition (Movie S2). In contrast, CIP4-KD cells were immobile, poorly dynamic, and did not start to break away from the cluster until 4 h after EGF addition and only completed scattering 11 h after EGF stimulation (Fig. 1E and Movie S2). We further quantified cell scattering by measuring the total distance travelled by cells from their original position within a colony. Removal of CIP4 reduced the scattering distance by ~80% compared with control cells (Fig. 1H). The increased cell compaction and delayed EGF-induced scattering of CIP4-KD cells suggests that CIP4 might affect the ability of epithelial cells to invade into the ECM, particularly under chemotactic stimulation with EGF. Consistently, CIP4 removal significantly impaired the invasive, EGF-dependent, chemotaxis of MCF10A cells into Matrigel-coated transwells (Fig. 1I).

To determine whether defective EGF-induced cell scattering of CIP4-KD cells was due to alterations in EGFR signaling or trafficking, we first evaluated the levels of EGFR expression. We detected no significant differences in total (in both sparse or confluent cells) or cell surface levels of EGFR among the cell lines tested (Fig. S2A and S2B). Similarly, CIP4 depletion did not significantly alter EGFR signaling as determined by measuring the levels of activated ERK1/2, AKT (Fig. S2C) and EGFR (Fig. S2F).

TOCA family members have been shown to control early events of EGFR CME and trafficking (Itoh et al., 2005). However, CIP4 depletion did not significantly alter the rates of EGFR endocytosis (Fig. S3D), recycling (Fig. S3D-E) or the extent of EGFR degradation (Fig. S2F). Thus, CIP4 is dispensable for EGFR signaling, stability and intracellular trafficking.

TOCA family members have also been shown to be essential for activation of N-WASP/WASP downstream of CDC42 in mammalian cells, as well as in *Drosophila*. However, removal of CIP4 did not alter EGF-mediated activation of N-WASP, monitored by measuring its tyrosine phosphorylation (Torres and Rosen, 2003) (Fig. S2G), suggesting that this latter pathway is not responsible for the increased cell cohesion following CIP4 silencing.

CIP4 controls cell scattering and cohesion by regulating EGF-induced actomyosin contraction

Epithelial cell scattering critically depends on modulation of junctional-localized actomyosin contractility (de Rooij et al., 2005). Indeed, time-lapse recordings of EGFP-E-cadherin dynamics during MDCK cell scattering revealed that tensile, orthogonal stresses build up along cell-cell junctions, until cells are abruptly pulled apart (de Rooij et al., 2005). We observed a similar dynamic behavior of junctional EGFP-E-cadherin during EGF-mediated scattering of MCF10A cells (Movie S3). Conversely, in CIP4-depleted cells, orthogonal tensile stress was insufficient to pull apart cell-cell junctions (Movie S3). This result suggests that CIP4 might regulate EGF-

dependent contractility at junctions. To test this possibility, we investigated the phosphorylation of the myosin II regulatory light chain (MLC), which is the main regulatory event leading to actomyosin contractility (Bresnick, 1999). EGF stimulation increased total levels of phosphorylated MLC (pMLC) and promoted the accumulation of pMLC adjacent to cell-cell junctions in control cells. Both these events were markedly diminished following CIP4 depletion (Fig. 2A and Fig. S4A). To verify that CIP4 removal causes cell compaction, at least in part, by impairing the localized accumulation of pMLC, and thus actomyosin contractility, we performed three additional sets of experiments. In the first approach, we took advantage of recent observations indicating that junctional E-cadherins act as mechanosensor devices (Borghi et al., 2012). We used a next generation Fo□rster resonance energy transfer (FRET)-based, E-cadherin tension sensor [EcadTSMod-CFP(E2)] to measure the magnitude of tensile forces transmitted through the cytoplasmic domain of E-cadherin in epithelial cells (Borghi et al., 2012) during scattering following stimulation with EGF. The EcadTSMod, is built by inserting in the cytoplasmic tail of E-cadherin the monomeric, aggregation-free variant of CFP(E2) fused to the N terminus of a protein domain from spider silk that functions as a nanospring and EYFP (Venus, A206K) fused to the C terminus (Borghi et al., 2012). Under conditions of low tension, the CFP(E2) and Venus are close enough to undergo FRET; however, when orthogonal tensile force is applied, the distance between the two fluorescent proteins increases and FRET decreases (Fig. 2B). Thus, the FRET signal responds to mechanical tension across E-cadherin molecule, such as those that develop as a consequence of EGF-mediated scattering. We transiently express EcadTSMod-CFP(E2) in scr-CTR and CIP4-KD and verify that is properly localizes along junction (Fig 2C). We further express an EcadTSModΔcyto-CFP(E2), as a control construct, which can no longer interact with the underlying actin cytoskeleton due to the lack of the β-catenin–binding domain, hence it is insensitive to actomyosin, tensile stresses (Borghi et al., 2012). Under EGF deprivation, both scr-CTR and CIP4-KD cells were compact, and display similar elevated E-cadherin FRET index at cell-cell junction. However, following EGF stimulation, the junctional FRET index significantly decreases in scr-CTR, but not in CIP4-KD (Fig. 2C-D and Movie S4). As expected, we detected no variation in FRET index when EcadTSModΔcyto-CFP(E2) was used (Fig. 2D). Thus, Loss of CIP4 prevents the accumulation of tension across junctional E-cadherin. As a second approach we exploited recent findings demonstrating that the mechanoresponse of E-cadherin is potentiated by vinculin, which is specifically recruited to anchor sites within AJs subjected to tensile stress in a myosin II- and actomyosin contractility-dependent fashion (le Duc et al., 2010). Consistently, we found that in control MCF10A cells, EGF induced accumulation of pMLC at adhesion sites, which was accompanied by the accumulation of vinculin (Fig. 2E). Conversely, little or no detectable vinculin accumulated at cell-cell junctions after removal of CIP4, mirroring the lack of pMLC

recruitment (Fig. 2E). Secondly, we reasoned that we should be able to rescue defective EGF-induced accumulation of pMLC at adhesion sites and cell scattering in CIP4-KD cells by enhancing cell contractility. Actomyosin contractility is dependent on cell adhesion onto the underlying ECM (Choquet et al., 1997; Danen et al., 2005; Ren et al., 1999). Furthermore, increased cell adhesion strength correlates with increased cell scattering (de Rooij et al., 2005). Hence, we tested whether plating cells on ECM that is known to activate integrin-mediated adhesion and actomyosin contractility, rescued defective cell scattering of CIP4-KD cells. MCF10A cells rapidly adhere and spread when plated onto fibronectin, but poorly adhere to laminin and vitronectin (Fig. S5A). CIP4 removal slightly delayed adhesion to fibronectin, but did not affect cell spreading, integrin-dependent activation of focal adhesion kinase (FAK; Fig. S5A-C), or the surface levels of total and active β1 and of total α5β1 integrins (Fig. S5D), despite a reduction in the internalization of β1 adhesion receptors (Fig. S5E). Remarkably, however, the cell scattering deficiency and cell cohesion of CIP4-KD cells were rescued upon plating cells onto fibronectin, but not onto laminin or vitronectin (Fig. 3A-B, Fig. S4B-D and Movie S5). This correlated with increased EGF-induced levels of total and junctional-localized pMLC (Fig. 3C and Fig. S4B). Collectively, these results suggest that CIP4 is required to promote optimal EGF-induced actomyosin contractility, which contributes to the generation of sufficient tension to break cell junctions apart and promote cell scattering.

CIP4 is required for E-cadherin internalization upon EGF stimulation

EGF stimulation promotes E-cadherin mobilization and disassembly (Durer et al., 2007). The increased cell cohesion resulting from CIP4 removal could partly be explained by a direct effect of CIP4-KD on E-cadherin expression. However, E-cadherin levels were not significantly different between control and CIP4-KD MCF10A cells (Fig. 4A). Alternatively, CIP4 might influence E-cadherin trafficking (Le et al., 1999). We initially examined in detail the dynamics of EGFP-E-cadherin after acute stimulation with EGF. EGFP-E-cadherin expressed in control cells initially localized at cell-cell junctions and in vesicular intracellular structures, likewise the endogenous protein (Fig. 4B). Stimulation with EGF promoted the mobilization of E-cadherin into vesicles (Fig. 4B). Depletion of CIP4 impaired E-cadherin internalization and prevented EGF-induced junctional disruption (Fig. 4B and Movie S3). Next, we sought to quantify E-cadherin internalization using a surface biotinylation and internalization assay. We observed, as expected, that a fraction of cell surface E-cadherin is rapidly internalized upon EGF addition to control MCF10A cells (Fig. 4C-D). Silencing of CIP4 (either alone or in conjunction with other TOCA family members) increase, instead, the levels of steady-state cell surface E-cadherin (Fig. 4C, lane ‘M’), consistent with augmented cell compaction and increased junctional localization of this

protein. Furthermore, EGF-induced internalization of E-cadherin was markedly reduced in CIP4-KD and 3KD cells compared to control MCF10A cells (Fig. 4C-D).

To corroborate these latter observations, we also employed HECD-1, an antibody that recognizes the extracellular domain of E-cadherin, to monitor EGF-induced internalization of E-cadherin (Fig. 4E and Fig. S6A). EGF induced a rapid internalization of E-cadherin, which was impaired by removal of CIP4. The extent and kinetics of E-cadherin endocytosis measured using the HECD-1 antibody were similar to those obtained using the biotinylation assay (compare Fig. 4E with 4D). Thus, CIP4 is required to promote EGF-induced E-cadherin endocytosis.

Collectively, our data indicate that CIP4 is a pivotal regulator of epithelial morphogenetic events that controls the amount of junctional E-cadherin through endocytosis and growth factor-induced, cell adhesion-dependent actomyosin contractility, thereby coordinating cell-cell adhesion in response to soluble stimuli.

CIP4 interacts with E-cadherin and SRC in MCF10A cells after EGF stimulation

To gain clues as to the molecular mechanisms underlying the role of CIP4 in EGF-dependent endocytosis of E-cadherin, we first assessed whether CIP4 intracellular localization was affected by EGF stimulation. Endogenous CIP4 is distributed primarily in the cytoplasm in EGF-deprived MCF10A cells (Fig. 5A). EGF stimulation promoted CIP4 localization at membrane ruffles (Fig. 5A), and induced a marked redistribution of CIP4 from the cytoplasm to cell junctions, where it partially, but evidently, co-localized with E-cadherin, suggesting that the two proteins might associate in a growth factor-dependent manner (Fig. 5A). Consistently, we confirmed a physical interaction between CIP4 and E-cadherin by co-immunoprecipitation, and observed that this interaction was enhanced by stimulation with EGF (Fig. 5B).

Another important regulator of E-cadherin signaling, trafficking and actomyosin contractility is the non-receptor tyrosine kinase SRC (Andreeva et al., 2014; Avizienyte et al., 2002; Fujita et al., 2002a; Palacios et al., 2005). Indeed, as previously shown (Canel et al., 2010), pharmacological inhibition of SRC family activity with PP2 or Dasatinib (Fig. S6B) significantly impaired E-cadherin endocytosis (Fig. S6C) and EGF-induced cell scattering (Fig S6D) both in control and CIP-KD cells. Interestingly, SRC has been shown to interact with and phosphorylate CIP4 (Dombrosky-Ferlan et al., 2003; Hu et al., 2011; Lock et al., 1998). Thus, we tested whether CIP4, in addition to interacting with E-cadherin, also interacts with SRC. We observed that endogenous SRC and CIP4 co-immunoprecipitated and that their interaction was enhanced by EGF stimulation (Fig. 5B), suggesting that CIP4 enters into a complex with E-cadherin and SRC. Removal of CIP4 significantly reduced the amount of E-cadherin co-immunoprecipitating with SRC following EGF stimulation, and inhibited EGF-induced SRC activation (Fig. 5C). Thus, CIP4

enters into and promotes the formation of an EGF-dependent E-cadherin/SRC complex, and controls SRC activation. We further characterized the nature of the SRC/CIP4 interaction using *in vitro* binding experiments. We found that the SH3 domain of SRC was sufficient to pull-down CIP4 (Fig 5D). Since SH3 domains typically bind to proline-rich regions, we performed a sequence analysis of CIP4 and identified a potential SH3 binding site encompassing amino acids 485-505. Deletion of the central P492 and P493 residues (ΔP-CIP4) markedly reduced the binding of CIP4 to the SRC SH3 domain (Fig. 5D). Notably, the interaction between the SRC SH3 domain and CIP4 was detectable only after stimulation of cells with EGF, confirming co-immunoprecipitation experiments (Fig. 5E). To demonstrate the functional relevance of the CIP4/SRC interaction, we reconstituted CIP4-KD cells either with siRNA-resistant WT- or ΔP-CIP4 mutant. Only the expression of WT-CIP4, but not of ΔP-CIP4 restored the cell compaction (not shown) and scattering phenotypes (Fig. 5F and Movie S6).

CIP4 facilitates TGF-ß1-induced mesenchymal morphological conversion of MCF10A cells

Endocytosis of E-cadherin also occurs during TGF-ß1-induced EMT (Miller and McClay, 1997). TGF-ß1 promotes permanent loss of cell adhesion by negatively regulating E-cadherin expression and by modulating dynamin-dependent endocytosis (Ogata et al., 2007; Zheng et al., 2009). We thus tested whether CIP4 is involved in TGF-ß1-induced scattering and junctional remodeling. TGF-ß1 stimulation induced scattering of control MCF10A cells, accompanied by the acquisition of a mesenchymal morphology (Fig. 6A). Depletion of CIP4 inhibited both of these TGF-ß1-induced effects, with CIP4-KD cells remaining as compacted clusters in the presence of TGF-ß1 (Fig. 6A).

To assess whether CIP4 is required for activation of the TGF-ß1-dependent transcriptional program that underlies EMT, we measured mRNA levels of the transcription factors, Snail1 and Snail2, which are hallmarks of EMT. The expression of these transcription factors was, as expected, regulated by TGF-ß1, and CIP4 removal had only a marginal effect on (Snail2), or delayed (Snail1), these responses, suggesting that CIP4 is not required for TGF-ß1 signaling leading to canonical EMT (Fig. 6B). Since TGF-ß1 also controls E-cadherin expression and promotes an E-cadherin/N-cadherin switch (Peinado et al., 2004), we next determined the total levels of these junctional proteins. While removal of CIP4 did not affect E-cadherin levels, N-cadherin expression was reduced in untreated CIP4-KD cells compared to control cells (Fig. 6C). However, stimulation with TGF-ß1 increased N-cadherin expression in both cell types to a similar extent, further suggesting that CIP4-depletion does not affect TGF-ß1 signaling (Fig. 6C). We therefore assessed whether removal of CIP4 influences TGF-ß1-induced E-cadherin endocytosis and found that this response was delayed in CIP4-KD cells (Fig. 6E-F). Notably, TGF-ß1 also caused a transient elevation of CIP4 mRNA that was accompanied by an increase in CIP4 protein (Fig. 6C-D), at a time coincident

with the onset of cell scattering. The delayed and transient peak of E-cadherin internalization observed after removal of CIP4 suggests that alternative and possibly redundant mechanisms of endocytosis might partially compensate for CIP4 deficiency. CIP4 depletion was also accompanied by impaired TGF-ß1-dependent SRC activation, which was short-lived compared with controls, suggesting that the CIP4-SRC axis is also involved in TGF-ß1-induced cell scattering (Fig. 6G).

Finally, since EMT is invariably associated with increased migratory and invasive properties, we pre-treated control and CIP4-KD cells with TGF-ß1 and determined their invasive ability through Matrigel^{TM}-coated transwells. Removal of CIP4 significantly impaired TGF-ß1-induced invasion both in the presence and absence of EGF (Fig. 6H). This result corroborates the importance of CIP4 in the remodeling of junctional E-cadherin required for epithelial cell plasticity.

Deregulation of CIP4 in human breast cancer

The critical role of CIP4 in the control of cell cohesion and cell invasion suggests that aggressive and invasive human breast cancers might positively select for elevated levels of this protein. To test this hypothesis, we analyzed formalin-fixed paraffin-embedded tissue samples of human breast cancer (BC) assembled on tissue microarrays (TMAs). These TMAs comprised 349 primary breast cancer samples from patients operated at the European Institute of Oncology (IEO) between 1994 and 1997 (Fig. S7A). CIP4 expression was evaluated by immunohistochemistry (IHC) using the anti-CIP4 antibody (Fig. 7A), the specificity of which was confirmed using control and CIP4-KD MCF10A cells (Fig. S7B). The level of CIP4 was significantly increased in BCs characterized by clinically aggressive prognostic factors (Fig. 7B), most notably negative estrogen receptor (ER; $P > 0.001$) and progesterone receptor (PgR; $P = 0.0014$) status, and positive ERBB2 status ($P = 0.0104$). In keeping with a role of CIP4 in the regulation of cell cohesion and cell invasion, its elevated expression was significantly associated ($P = 0.0046$) with disease relapse (distant metastasis, local relapse or death from breast cancer). Notably, in ER- and PgR-positive, as well as in ERBB2-negative tumors, which usually have a good prognosis, elevated expression of CIP4 was still significantly associated with disease recurrence (Fig. 7C). Moreover, in Grade 2 (G2) breast tumors, which are associated with an intermediate risk of recurrence, CIP4 overexpression was associated with poor outcome ($P = 0.0146$). Multivariate analysis corroborated this finding revealing that CIP4 expression is an independent predictor of poor prognosis, with an odds ratio (OR) of 2.413 (CI: 1.007-6.021, $P = 0.0482$) of disease relapse (Fig. 7D). Although an analysis of a larger cohort of primary, and possibly metastatic, tumors is necessary to gain a complete picture of the clinical significance of CIP4 overexpression, our TMA analysis provides statistically significant evidence in support of our conclusion that CIP4 is positively associated with highly aggressive, metastatic, ERBB2-positive breast cancers.

CIP4 is required for ERBB2-induced invasive outgrowth of mammary epithelial cells and for the conversion from breast ductal carcinoma *in situ* to invasive carcinoma

To test whether CIP4 is involved in promoting invasive behavior and local dissemination, we employed various *in vitro* and *in vivo* model systems of breast cancer invasion. CIP4 levels are elevated in aggressive ERBB2-positive tumors. Thus, we generated stable CIP4-KD MCF10A cells expressing inducible ERBB2 [MCAF10A.ERBB2; (Muthuswamy et al., 2001)]. Removal of CIP4 did not affect ERBB2 levels or activation, rather it slightly increased ERBB2 phosphorylation after stimulation with the dimerizer AP1510 (Fig. 8A). However, CIP4 removal diminished Matrigel invasion by more than 3-fold in response to ERBB2 activation (Fig. S8A).

Next, we tested the effect of CIP4 depletion on invasion of MCF10A.ERBB2 cells into a three-dimensional basement membrane matrix. Consistent with published data (Seton-Rogers et al., 2004), untreated MCF10A.ERBB2 cells formed acini with disrupted (multi-acinar) morphology (Fig. 8B). Following activation of either ERBB2 or TGF-β1 receptors, MCF10A.ERBB2 cells extended rare and poorly invasive protrusions, which, however, became more frequent and highly invasive upon concomitant stimulation of both receptors (Fig. 8B). Removal of CIP4 robustly prevented both the formation of rare protrusions in single agent-treated cells, and severely reduced invasive growth of activated MCF10A.ERBB2 in the presence of TGF-β1. In constrast, in the absence of stimuli, CIP4 depletion had no obvious effects on acini formation and morphology or growth rates (Fig. 8B and data not shown), consistent with its primary role in controlling cell cohesion and growth factor-dependent cell-cell junctional dynamics. We also stably silenced CIP4 in HCC-1954 cells, which are poorly differentiated, highly metastatic ERBB2-positive breast cancer cells (Gazdar et al., 1998) that display elevated endogenous levels of CIP4 (Fig. S8B). Removal of CIP4 in these cells increased cell compaction (Fig. S8C-D) and reduced cell invasion (Fig. S8E).

Finally, we investigated whether CIP4 is required for the initial local dissemination, invasion and conversion from a DCIS to IDC. To this end, we stably removed CIP4 in a MCF10A cell derivative, MCFA10.DCIS.com (Fig. 8C). These cells have been extensively characterized as an experimental model of human DCIS, which forms comedo DCIS-like lesions that spontaneously progress to IDC (Hu et al., 2008; Miller et al., 2000). Depletion of CIP4 in these cells had no effect on cell growth (data not shown), but promoted cell compaction (Fig. 8D), impaired HGF-induced invasive outgrowth into a three-dimensional basement membrane matrix (Fig. 8E), and severely delayed the DCIS-to-IDC conversion in immunocompromised mice (Fig. 8F). Indeed, MCFA10.DCIS.com control cells formed typical *in situ* carcinoma surrounded by a well-defined and continuous layer of myoepithelial cells (positive for alpha smooth muscle actin), which however was lost 3 weeks after injection, indicative of the acquisition of a highly invasive

phenotype (Fig. 8F). Depletion of CIP4 impaired this DCIS-to-IDC conversion (Fig. 8F), but had no effect on tumor size or growth (data not shown). Thus, CIP4 is required for invasion of ERBB2-positive breast cancer and its removal delays DCIS-to-IDC conversion.

Discussion

Regulation of epithelial morphogenesis, differentiation and function critically depend on the dynamic remodeling of E-cadherin–mediated adhesion (Halbleib and Nelson, 2006). Perturbation of epithelial cell-cell junctions and cell-ECM adhesion results in acquisition of mesenchymal characteristics, with increased proliferation and motility (D'Souza-Schorey and Chavrier, 2006; Lozano et al., 2003). Thus, appropriate control of cell adhesion is important for many aspects of epithelial function in health and disease. Our findings unveil a specific, non-redundant role of the TOCA family member, CIP4, in the regulation of cell-cell junction stability and cell-ECM adhesion during mammalian epithelial morphogenetic events.

Endocytosis is a coordinated, spatio-temporal process that requires deformation of the plasma membrane. Through their SH3 and F-BAR domains, members of the TOCA family have the potential to act in a diverse range of internalization processes. Indeed, all the members of this family have been shown to promote actin assembly and to regulate CME, in a redundant fashion, in different model systems (Fricke et al., 2009; Giuliani et al., 2009; Ho et al., 2004). However, there is growing evidence for unique functions of individual TOCA family members. For example, using CIP4 knockout mice, a recent study revealed a unique role of CIP4 in macropinocytosis, indicating that CIP4 is not restricted to CME, but also affects other modes of endocytosis (Feng et al., 2010). In addition, novel roles of CIP4 have recently been described in neuronal development (Saengsawang et al., 2012) and in B cell lymphomas (Malet-Engra et al., 2013). In neurons, where other TOCA family members are also expressed (Wakita et al., 2011; Wu et al., 2010), CIP4 has no effect on endocytosis, but rather inhibits neurite extension by promoting the formation of lamellipodial protrusions.(Malet-Engra et al., 2013) CIP4 has also been shown to regulate the formation of podosomes in primary macrophages (Linder et al., 2000) and invadosomes in breast tumor cells (Hu et al., 2011; Pichot et al., 2010). Together, these studies point to a critical role of CIP4 as a regulator of cell invasion. Our findings support in part this notion, by establishing that CIP4 controls migration of epithelial cells indirectly by modulating cell cohesion through its “canonical” endocytic function, rather than by impairing migratory parameters. This endocytic role is uniquely exerted by CIP4 and not by the other members of the TOCA family, despite their involvement in CME (Frost et al., 2008; Itoh et al., 2005; Taylor et al., 2011; Wu et al., 2010), indicating that functional specificity is likely determined by the type of cargo being internalized. It is noteworthy that we found that EGF stimulation, which acts as a potent motogenic factor in mammary epithelial cells, promotes the relocalization of CIP4 to E-cadherin junctions, where internalization of this latter protein is initiated. We also observed that EGF causes the re-localization of the protein to extending lamellipodia and ruffles along the protrusive leading edges, similarly to what has been reported in neurons (Saengsawang et al., 2012). Hence, CIP4 might be critical to

coordinate junction disassembly, through endocytosis, with the formation of migratory protrusions, leading ultimately to a mesenchymal mode of motility and cell invasion. This latter contention is consistent with our observation that the expression of CIP4, but not TOCA-1 or FBP17, is increased in invasive breast cancer cell lines in comparison with weakly or non-invasive breast cancer cell lines (Hu et al., 2011; Pichot et al., 2010).

Several mechanisms that regulate the availability of E-cadherin for the formation of cell-cell junctions have been proposed over the years. A focal event is the endocytosis and sorting of internalized E-cadherin to either degradation or recycling pathways (Bryant and Stow, 2004). In this respect, Rho family GTPases, and most notably CDC42, regulate not only the formation of AJs (Kim et al., 2000), but also their dynamic remodeling during tissue rearrangement by controlling multiple steps of E-cadherin trafficking (Baum and Perrimon, 2001). In the neuroectodermal epithelium of *Drosophila*, for example, CDC42 and PAR proteins were shown to regulate the trafficking of AJ components and apical polarity proteins to maintain AJ stability in the face of cell rearrangements (Harris and Tepass, 2008). In this system, CDC42, together with the PAR complex, is required to decrease the endocytic uptake of apical proteins and to promote the progression of apical cargo from the early to the late endosome. Conversely, in the developing pupal notum or dorsal thorax of the fly, CDC42 functions with PAR6/aPKC and CIP4/N-WASP to regulate early events in E-cadherin endocytosis, mimicking the phenotype obtained after loss-of-function of the GTPase dynamin (Georgiou et al., 2008; Leibfried et al., 2008). Therefore, in most epithelial tissues of the fly, the apical polarity complex CDC42–PAR6–aPKC seems to induce the local activation of TOCA family proteins to drive dynamin-mediated endocytosis of AJ material and the recycling of E-cadherin complexes. In mammary epithelial cells, however, CIP4 is fully dispensable in mediating the activation of a CDC42/N-WASP, a function likely fulfilled by the other members of the family. CIP4 is, instead, essential for the formation of a macromolecular complex that includes E-cadherin and SRC. SRC is a central regulator of signaling downstream of EGFR and has been shown to regulate EMT by disrupting AJs (Canel et al., 2013). Mechanistically, SRC can alter E-cadherin trafficking by redirecting E-cadherin from a recycling pathway to a lysosomal-targeting pathway. This rerouting can be achieved by direct, SRC-mediated tyrosine phosphorylation of E-cadherin cytoplasmic tails, which marks E-cadherin for ubiquitination and subsequent delivery to lysosomal degradation (Fujita et al., 2002b). However, we showed that CIP4 removal, despite diminishing EGF-induced activation of SRC and its association with E-cadherin, does not affect E-cadherin phosphorylation (data not shown) or its rate of degradation, suggesting that CIP4 is not essential for this late trafficking step. CIP4 may, instead, act during the early events of endocytosis, where its ability to curve the plasma membrane might facilitate the invagination of newly formed, presumably clathrin-coated, pits. How SRC fits into this scenario remains, however, to be firmly

established. Interestingly, (Avizienyte et al., 2002; Canel et al., 2013; Canel et al., 2010; Wang et al., 2011)one pathway that is activated downstream of SRC involves ROCK kinase and leads to the regulation of actomyosin-dependent junctional contractility (Andreeva et al., 2014), Furthermore, evidence is accumulating of tight interplay between actomyosin contractility and E-cadherin endocytosis during epithelial morphogenesis (Levayer et al., 2011). Within this context, CIP4 may serve as key molecular hub in interconnecting the two processes, which ultimately impact on epithelial cell cohesion, motility and invasion.

In summary, while further work is required to address the precise molecular mechanisms underlying CIP4 function in cell:ECM adhesion, our data establish the unique relevance of this endocytic F-BAR-containing protein in mediating, through regulation of cell cohesion, epithelial cell motility and invasive ability.(Lodhi et al., 2007). It is therefore not surprising that CIP4 elevation is associated with increased disease relapse of ERBB2-positive breast cancer. In this setting, high levels of CIP4 may have been selected to reduce cell cohesion and cell-cell interaction and promote dissemination. Remarkably this pro-metastatic role of CIP4 is not limited to this subset of breast cancer, pointing to a key and essential role of this F-BAR protein in the regulation of breast cancer metastasis.

Experimental Procedures

Cell motility and adhesion assays

Random migration of MCF10A cells was monitored under normal growth conditions. Briefly, cells were seeded ($1x10^4$ cells/well) in a 6-well plate and maintained in complete medium for 2 days. Cell motility was monitored at 37°C over a 24-hour period. Pictures taken every 15 minutes, from 20 different positions using an Olympus ScanR system equipped with a Hamamatsu ER camera. Cell tracking was performed by using the "Manual tracking" and "Chemotaxis and migration tool" plug-in distributed by ImageJ software.

EGF-induced MCF10A cell scattering. Cells ($1x10^5$ cells/well, in a 6-well plate) were EGF-starved for 24 hours and stimulated with 100 ng/ml EGF to initiate cell scattering. Scattering was monitored for 24-hour. Alternatively, EGF-induced scattering assay was monitored by taking pictures at fixed time points.

Cell attachment to the substrate was measured using the xCELLigence system. Shortly, a 96 well plate containing an array of microelectronic sensors (Roche) was coated with 100 µg/ml poly-D-lysine, 10 µg/ml fibronectin, 5 µg/ml vitronectin or 10 µg/ml laminin overnight at 4^o C and incubated 1 hour with heat-inactivated 5% BSA prior seeding cells.

Statistical analysis

Cell biology: differences between experimental groups were examined for statistical significance using the paired Student's *t*-test (**P*<0.05, ***P*<0.01 and ****P*<0.001). Data are expressed as mean ± s.e.m..

TMA tumor sections: differences between experimental groups were examined for statistical significance using the paired Student's *t*-test. Where applicable, data are expressed as average ± s.e.m. TMA data analysis were performed using JMP 10.0 statistical software (SAS Institute, Inc). The association between CIP4 expression and clinicopathological parameters was evaluated using the Pearson chi-square test. For univariate and multivariate analysis, Odds ratio (OR) and 95% Confidence Intervals were obtained from the logistic regression model.

MTT proliferation assay

Cells were seeded at $1x10^3$ cells/well in 96-well plates and cultured for 36 hours in complete medium. Cells were then washed with PBS and 500 µg/ml MTT (3-(4,5-dimethylthiazol-2-yl)-2,5-diphenyltetrazolium bromide; Sigma-Aldrich) was added to each well. After 2 hours of incubation at 37°C, the MTT solution was removed and 100 µl of DMSO was added to each well. The absorbance was measured at 570 nm using a VICTOR3™ V Multilabel Counter model 1420 from PerkinElmer.

E-cadherin internalization

Scr-CTR and CIP4-KD MCF10A cells were transfected with human E-cadherin-GFP (addgene) using Amaxa® Nucleofector® (Lonza) and seeded ($1x10^5$) in glass bottom 22 mm diameter dishes (WillCo-dish®). After 24 hours, cells were EGF-starved for a further 24 hours before stimulating with 100 ng/ml EGF. E-cadherin-GFP internalization was then monitored for 4 hours at 37°C. Fluorescence microscopy was performed on an UltraVIEW VoX (Perkin Elmer) spinning disk confocal unit, equipped with an EclipseTi inverted microscope (Nikon), a C9100-50 emCCD camera (Hamamatsu) and driven by Volocity software (Improvision, Perkin Elmer). GFP signals and DIC (differential interference contrast) images were acquired with a 60X oil immersion objective (NA 1.4) as Z-stacks (0.7 micron step).

For HECD-1 anti-E-cadherin internalization, cells were grown on glass coverslips and EGF-starved for 24 hours before experiments. Samples were then incubated for 1 hour at 4°C with anti-E-cadherin (HECD-1) IgG diluted in PBS solution. Where appropriate, cells were pre-treated for 12 hours with 10 µM PP2 inhibitor before incubation with the HECD-1 antibody. Coverslips were washed with ice-cold PBS to remove the unbound antibody and the media was replaced with pre-warmed culture medium containing 100 ng/ml EGF and 5% horse serum. After incubation at 37°C

for various lengths of time, cells were washed with PBS and returned to 4°C. The residual surface-bound antibody was removed by acid washing (0.5 M acetic acid, 0.5 M NaCl). Cells were washed with PBS before fixation with 4% paraformaldehyde for 10 minutes at room temperature. Indirect immunofluorescence staining was performed on permeabilized cells by incubating with CY3-conjugated anti-mouse antibody and FITC-conjugated phalloidin. Internalization of E-cadherin was quantified using the particle analysis tool of ImageJ software.

Surface biotinylation assays

The cell surface was labeled for 30 minutes on ice with 0.5 mg/ml biotin (EZ-Link^{T}M Sulfo-NHS-SS-Biotin) in PBS pH 7.4. After quenching with 0.15% glycine in PBS pH 7.4 for 5 minutes, cells were incubated in complete growth medium supplemented with 100 ng/ml EGF at 37°C for 2 hours. At different time points, cells were removed from the incubator, put on ice, washed with cold MESNA buffer (150 mM NaCl, 1 mM EDTA, 0.2% BSA, 20 mM Tris –HCl pH 8.6, 50 mM MESNA) to remove cell surface biotin and lysed. For surface E-cadherin level determination, labeled cells were directly lysed after the quenching step (designated as M). As a negative control (-), cells were directly treated with MESNA buffer after the quenching step without incubation at 37°C. Biotin-labeled proteins were then precipitated using streptavidin-agarose beads and subjected to immunoblotting with the anti-E-cadherin antibody. Actin levels were used to normalize input protein amounts between different conditions and cell lines.

Internalization and recycling assays

^{125}I-EGF surface levels, internalization and recycling assays were performed exactly as described(Sorkin and Duex, 2010)

Internalization of total and active β1 integrin was assessed as in (Roberts et al., 2001).

Additional details are in the Supplemental Experimental Procedures.

FRET live microscopy and analysis

EGF-deprived scr-CTR and CIP4-KD MCF10A cells microinjected with either EcadTSModWT or EcadTSModΔCyto constructs, were stimulated with EGF (100 ng/ml) to induce scattering. FRET imaging was performed on a Delta Vision Elite system (Applied Precision) equipped with a Photometrics CoolSNAP HQ2 CCD Camera and an UPLSApo 60x (1.42 NA) oil immersion objective (Olympus). The system is coupled with an environmental chamber maintained at 37°C in an atmosphere of 5% CO2. To monitor the biosensor FRET changes a simple ratiometric approach was used, as previously described (Aoki and Matsuda, 2009). Briefly, CFP(E2) (ex: 438/24nm, em: 470/24nm), FRET (ex: 438/24nm, em: 559/38nm) and Venus (ex: 513/17nm, em: 528/38nm) channels were collected in sequence. Using an in-house macro in ImageJ, images were background corrected, realigned, converted in 32 bits, smoothed and the Venus channel was thresholded and used as a binary mask as described in (Kardash et al., 2011)The average FRET/CFP ratio was then calculated over the cell-cell contacts.

Wound healing assays

MCF10A scr-CTR and CIP4-KD cells were seeded at 5x10^{5} cells/well in 6-well plates and cultured until a uniform monolayer had formed. Wound area was made using a sterile 10 µl pipette tip, and washed extensively with PBS. The closure of the wound was then monitored at 37°C and 5% CO_2 by time-lapse analysis over a 24-hour period, with pictures taken every 5 minutes. Images were taken of 5 fields of views, for duplicate samples, with an inverted microscope Olympus ScanR using the 10X objective. Cell-free area was calculated for each cell line using ImageJ software.

Flow cytometric analysis

Expression of the integrins at the cell surface was analysed by flow cytometry as follow. Briefly, 5 x 10^{5} were incubated with mouse anti-integrin a5β1 or β1 for 1 h on ice, and then incubated with the secondary antibody for 1 h on ice. After the incubation cells were fixed with 4% PFA for 10 min on

ice. FACS data were acquired with the FACSCanto (Becton Dickinson) flow cytometer. Analysis were performed using FlowJo version 4.6.2 (Treestar).

Three-Dimensional morphogenesis of mammary epithelial cell.

The details of 3D morphogenesis assay were described previously in (Debnath et al., 2003).

DCIS-to-IC conversion in NOD SCID gamma mice.

All animal experiments were performed in accordance with national and international laws and policies. Mice were bred and housed under pathogen-free conditions in our animal facilities at Cogentech Consortium at the FIRC Institute of Molecular Oncology Foundation and at the European Institute of Oncology in Milan.

DCIS-to-IC conversion in NOD SCID gamma mice. Scr-CTR and CIP4-KD MCF10.DCIS.com (100,000 cells) were injected subcutaneously into 6- to 9-week-old female NOD.Cg-Prkdc^{scid}Il2rg^{tm1Wjl}/SzJ [commonly known as the NOD SCID gamma (NSG)] mice in 50% Matrigel (BD Biosciences, Bedford, MA) as described (Hu et al., 2008). One to three weeks later xenografts were measured using digital calipers and tumor volume was calculated according to the formula: $L \times W^2/2 = mm^3$. The tumors were excised, fixed in 4% phosphate-buffered formalin and embedded in paraffin for IHC staining. The Scan Scope XT device and the Aperio Digital pathology system software (Aperio) were used to capture IHC images.

Figure legends

Figure 1: CIP4 regulates MCF10A cell compaction and EGF-induced scattering.
(**A**) Efficiency of TOCA family member knockdown in MCF10A cells assessed by immunoblotting (IB) with the indicated antibodies (abs) of lysates of shRNA-lentivirally infected MCF10A cells: scrambled shRNA (scr-CTR); shRNAs against CIP4 (CIP4-KD #1/#2), TOCA-1 (TOCA1-KD) or FBP17 (FBP17-KD) alone or together (CIP4/TOCA-1 double KD - 2KD; CIP4/TOCA-1/FBP17 triple KD - 3KD).
(**B**) Phase contrast images of various MCF10A cell lines growing in complete medium. Magnified view of the boxed area is shown. Bar, 1000 µm.
(**C**) The % of single cells or clusters relative to the scr-CTR MCF10A cells (n = 200 cells/genotype in 3 independent experiments). ****P*<0.001, t-test.
(**D**) Expression levels of CIP4 by IB in scr-CTR and CIP4-KD MCF10A cells expressing an shRNA-resistant CIP4 mutant (resCIP4-GFP) or an empty GFP vector (eGFP).
(**E**) Images of CIP4-KD#1 MCF10A cells expressing GFP or resCIP4-GFP. Left panels show low-magnification of GFP- or resCIP4-expressing CIP4-KD. Bar, 100 µm. Right, merged images of GFP epifluorescence (green), F-actin (red) and DAPI nuclei (blue). Bar, 20 µm.
(**F**) The number of single and clustered cells was quantified as in C (*n*=226 to 647 cells). ****P*<0.001, t-test.
(**G-H**) Still images of scr-CTR and CIP4-KD#1 MCF10A cells induced to scatter by adding EGF (100 ng/ml) to EGF-starved cells (see Movie S2). Cell scattering was quantified either (right graph) by determining the time required to complete scattering or (**H**) by tracking individual cells, measuring the accumulated distance covered by cells during four 4 h after EGF stimulation. Data is the % of accumulated scattering cell distance with respect to control cells (n = 25 cells/experiment in 4 experiments). ****P*<0.001, t-test.
(**J**) Invasion through Matrigel^{TM}-coated transwells toward EGF was assessed for 24 h. Representative images are shown. Cell invasion is the % of invasive cells with respect to control cells. ***P*<0.01, t-test.

Figure 2: CIP4 controls EGF-induced actomyosin tensile junctional stress across E-cadherin..
(**A**) *Left panels*, lysates of scr-CTR and CIP4-KD MCF10A cells treated with EGF (100 ng/ml) were IB with the indicated abs. *Right panels*, EGF-deprived scr-CTR and CIP4-KD #1 MCF10A cells plated on plastic were stimulated with EGF and stained with the anti-pMLC abs or phalloidin to detect F-actin. Arrows indicate pMLC at junctions. Bar, 25 µm.
(**B**) Scheme of E-cadherin tensor sensor
(**C**) Representative images from Movie S4 showing the FRET:CFP(E2) ratio of scr-CTR and CIP4-KD-MCF10A cells expressing the EcadTsMod-CFP(E2) and induced to scatter by EGF addition. The upper and lower limits of the FRET:CFP ratio range are shown on the left in the Ratio colored key (ImageJ software). CIP4-KD cells appear smaller due to compaction. Bar, 10 µm.
(**D**) Normalized FRET ratio at cell-cell junction of MCF10A cells treated as in (C). For each cell-cell contact, data were normalized to the FRET/CFP(E2) ratio value at time 0h. Data are expressed as mean ± s.e.m. (n = 30 cell-cell contacts/experiment, 3 experiments). *P<0.05, **P<0.01, t-test.
(**E**) EGF-deprived scr-CTR and CIP4-KD#1 MCF10A cells plated on plastic were stimulated with EGF and stained with the anti-Vinculin abs or phalloidin to detect F-actin. Arrows indicate vinculin. Bar, 20 µm.

Figure 3. Fibronectin adhesion rescues delayed scattering and reduces junctional actomyosin contractility.
(**A**) Control and CIP4-KD MCF10A cells were plated on plastic (uncoated) or fibronectin (FN) for 24 h. Cells were EGF-starved and stimulated with EGF to induce scattering. Representative images are shown. Graph on the left represents the time to reach complete scattering (****P*<0.001 compared to scr-CTR cells). Bar, 20 µm.

(**B**) Cell scattering was also quantified as described in Fig. 2D. *Left*, exemplar tracks of individual cells undergoing scattering. The accumulated scattering distance is expressed as the % of scr-CTR (n = 25/experiment, 3 experiments). ***P*<0.01, compared to scr-CTR MCF10A cells.
(**C**) *Left panels*, lysate of scr-CTR and CIP4-KD#1 MCF10A cells plated on fibronectin were IB for indicated abs. *Right panels*, EGF-deprived scr-CTR and CIP4-KD#1 MCF10A cells plated on FN were stimulated with EGF and stained with the anti-pMLC abs or phalloidin to detect F-actin. Arrows indicate pMLC at junctions. ****P*<0.01, compared to scr-CTR MCF10A cells. Bar, 25 μm.

Figure 4: CIP4 is required for the internalization of E-cadherin upon EGF stimulation.
(**A**) Lysates of scr-CTR or MCF10A cells devoid of TOCA family members and grown in complete medium were immunoblotted (IB) to detect E-cadherin.
(**B**) Internalization of E-cadherin-GFP upon acute EGF stimulation of EGF-starved MCF10A cells. Still images are from Movie S4.
(**C**) Surface biotinylation of MCF10A cells was as described in Experimental Procedures. Internalization of E-cadherin upon stimulation with EGF for up to 120' at 37°C. Surface levels of biotinylated E-cadherin is shown for unstimulated cells maintained at 4°C (M, membrane) and after washing with MESNA buffer (-, negative control). IBs in the lower panel show E-cadherin and actin in cell lysates used to perform biotin pull-downs.
(**D**) Quantification of internalized E-cadherin from the biotinylation assay expressed as % of cell-surface E-cadherin levels (n= 3 experiments).
(**E**) Internalization of surface-labeled E-cadherin using anti-E-cadherin (HECD-1) abs. We quantified the relative levels of internalized E-cadherin by evaluating total fluorescence intensity normalized for cell number and field area.

Figure 5: EGF induces redistribution of CIP4 to junctions and its interaction with E-cadherin and SRC in MCF10A cells.
(**A**) EGF-deprived MCF10A cells were stimulated with EGF for 5' at 37°C, fixed and stained to detect CIP4 (red) and either F-actin or E-cadherin (green). Insets are higher magnification of boxed areas. Bar, 20 μm.
(**B**) MCF10A cells were EGF-starved for 18 h and mock treated (-) or stimulated with EGF (+) for 30' at 37°C. Total cell lysates (TCLs, 1 mg) were immunoprecipitated with anti-CIP4 antibody or irrelevant IgG. TCLs (60 μg) and immunoprecipitates (IPs) were IB with the indicated abs.
(**C**) Lysates of control (scr-CTR) or CIP4-KD MCF10A cells, treated as in **B**, were immunoprecipitated with anti-SRC abs. IPs were IB with the indicated abs. Relative intensity of the pSRC signal with respect to total SRC (n = 3).
(**D**) Lysate of EGF-stimulated WT- or ΔP-CIP4-293T cells stimulated with EGF (100 ng/ml) incubated with GST- or GST-SH3 domain-bound to bead of SRC. Input and bound material were immunoblotted with the anti-CIP4 antibody. As control GST-SH3 beads were also incubated with lysate buffer alone (no lysate).
(**E**) EGF-deprived flag-tagged WT- or ΔP-CIP4-293T cells were stimulated with EGF for 30'. Lysates were incubated with equimolar amounts of GST or GST-SH3 domain of SRC, immobilized on glutathione beads. Input and bound material were immunoblotted with the anti-CIP4 antibody.
(**F**) scr-CTR and CIP4-KD #1 MCF10A were lentivirally infected with either an empty vector or with vector encoding siRNA-resistant WT-(resCIP4-WT) or ΔP-CIP4 (resCIP4-ΔP) mutants. Still images of lentivirally infected MCF10A cells induced to scatter by adding EGF (Movie S8). Scale Bar,100 μm. *Right, top panels*, CIP-WT and CIP4-ΔP were detected by IB with the indicated abs. Cell scattering, quantified as in Fig. 1G-H, is the % of accumulated scattering cell distance with respect to the distance of control cells (n = 55 cells/experiment in 3 experiments).***P*<0.01 compared to scr-CTR MCF10A cells, t-test.

Figure 6: CIP4 facilitates TGF-β1-induced mesenchymal morphological conversion in MCF10A cells.

(**A**) Phase contrast images of scr-CTR and CIP4-KD#1 MCF10A cells treated with 5 ng/ml TGF-β1 or vehicle for 24 h.
(**B**) QRT-PCR of the mRNA of indicated genes from scr-CTR and CIP4-KD MCF10A cells treated with TGF-β1 or vehicle. Data are the fold-increase with respect to vehicle treatment (1.5 h) for each cell sublines normalized for the 18S mRNA levels.
(**C**) Lysates of scr-CTR and CIP4-KD MCF10A cells treated with TGF-β1 (5 ng/ml) or vehicle (V) were IB with the indicated abs. The relative intensity of the N-cadherin with respect to vehicle-treated scr-CTR cells was quantified from 3 experiments. Long (l. exp) and short (s.exp) exposures of CIP4 IB.
(**D**) Total RNA was extracted from control MCF10A cells treated with TGF-β1 or vehicle, and CIP4 gene expression was measured by quantitative RT-PCR as described previously.
(**E**) Internalization of surface-labeled E-cadherin using an anti-E-cadherin (HECD-1) antibody.
(**F**) Relative levels of internalized E-cadherin were quantified by evaluating total fluorescence intensity and normalized with respect to cell number and field area (in μm^2).
(**G**) Total cell lysates of scr-CTR and CIP4-KD MCF10A cells treated with TGF-β1 (5 ng/ml) or vehicle (V) for the indicated time were IB with the indicated abs.
(**H**) Invasion assay of scr-CTR and CIP4-KD MCF10A cells pre-treated with TGF-β1 (5 ng/ml) or vehicle for 24 h, done as described in Fig. 1J. Cell invasion is the % of invasive cells with respect to control cells. **P*<0.05, ***P*<0.01 (compared to scr-CTR MCF10A cells pre-treated with vehicle), t-test.. Images of invaded cells are shown. Bar, 100 μm.

Figure 6. Deregulation of CIP4 in human breast cancer.
(**A**) CIP4 expression was measured by IHC on TMA. Example of CIP4 score assignment: CIP4 high expression was defined when tumors display an expression score >1. In tumor tissues the IHC signals were associated with the tumor cell and not with the stroma.
(**B-C)** Correlation of CIP4 expression with clinico-pathological parameters. The number of scored cases is lower than the total number of cases (349) since: i) in some cases, individual cores detached from the slides during the manipulations; ii) clinical information was not available for all patients.
(**D**) CIP4 overexpression is predictive of high risk of any breast-related event. Any Event: loco-regional relapse, distant metastasis, contralateral breast cancer or death for breast cancer; Distant Relapse: distant metastasis.

Figure 7: CIP4 is required for ERBB2-induce invasive outgrowth in mammary epithelial cells and DCIS-to-IDC conversion *in vivo*.
(**A**) Lysates of lentivirally-infected scr-CTR or CIP4-KD#2 MCF10A.ERBB2 cells were immunoblotted with the indicated abs. ERBB2 IPs were immunoblotted with anti-tyrosine abs.
(**B**) Phase-contrast micrograph of 7-day acinar structures of scr-CTR and CIP4-KD MCF10A.ERBB2 cells in the presence of TGF-β1 (5 ng/ml), AP1510 (100 nM), or both TGF-β1 (5 ng/ml) and AP1510 (100 nM). Bar, is 400 μm. The number of invasive acini is expressed as % of total acini ± s.e.m. (n = 30, 3 experiments).
(**C**) Lentivirally-infected scr-CTR or CIP4-KD#2 MCF10.DCIS.com cells were IB with the indicated abs.
(**D**) An equal number of scr-CTR and CIP4-KD0MCF10.DCIS.com cells were plated sparsely in complete medium. Phase-contrast images are shown. Right, magnified view of the boxed area. Bar, 250 μm. The % of single cells or clusters relative to the total number of MCF10.DCIS.com cells was quantified by counting at least 300 cells/genotype in 3 independent experiments. ***P*<0.01 compared to scr-CTR cells in clusters, t-test.
(**E**) Phase contrast micrograph of 9-day acinar structures of scr-CTR and CIP4-KD MCF.DCIS.com cells in the absence or presence of HGF (20 ng/ml). Bar, 400 μm. Quantification of invasive structures/cell acini is expressed as a % of total acini (n = 52 in 2 independent experiments).
(**F**) scr-CTR and CIP4-KD MCF10.DCIS.com cells were injected subcutaneously into NSG mice. Histological (H&E) and immunohistochemical analyses of scr-CTR and CIP4-KD

MCF10.DCIS.com xenografts were performed at 1 and 3 weeks after cell injection. H&E micrographs are shown at two different magnifications. The conversion from DCIS to IDC was detected in control xenografts between 1 and 3 weeks by loss of αSMA-positive myoepithelial layers. Images are representative of 3 independent experiments, where n = 5 mice/experimental condition. Bar, 100 μm.

Acknowledgments
We thank Rosalind Gunby for critically reading and editing the manuscript, Veronica Algisi for technical assistance on EGFR internalization; Senthil Muthuswamy for MCF10.p752 cell line. Y.R. is the recipient of Postdoctoral Training award from FRQS (Fonds de recherche du Québec - Santé); C.M. and P.M. were supported by fellowships from Fondazione Umberto Veronesi (FUV). This work was supported by grants from the Associazione Italiana per la Ricerca sul Cancro (AIRC,#10168 to GS) and (START UP program to LL), the Italian Ministries of Education-University-Research (MIUR-PRIN- 2009X23L78) and of Health, from AICR (International Association For Cancer Research –AICR- 09-0582 to GS and to LL), from the CARIPLO Foundation (#2010-0737); from the European Research Council (#268836) to G.S; the Fondazione Piemontese per la Ricerca sul Cancro - ONLUS – Intramural Grant 5X1000 2008 (LL).

References

Andreeva, A., Lee, J., Lohia, M., Wu, X., Macara, I.G., and Lu, X. (2014). PTK7-Src signaling at epithelial cell contacts mediates spatial organization of actomyosin and planar cell polarity. Dev Cell *29*, 20-33.

Aoki, K., and Matsuda, M. (2009). Visualization of small GTPase activity with fluorescence resonance energy transfer-based biosensors. Nat Protoc *4*, 1623-1631.

Aspenstrom, P. (1997). A Cdc42 target protein with homology to the non-kinase domain of FER has a potential role in regulating the actin cytoskeleton. Curr Biol *7*, 479-487.

Avizienyte, E., Wyke, A.W., Jones, R.J., McLean, G.W., Westhoff, M.A., Brunton, V.G., and Frame, M.C. (2002). Src-induced de-regulation of E-cadherin in colon cancer cells requires integrin signalling. Nature cell biology *4*, 632-638.

Balklava, Z., Pant, S., Fares, H., and Grant, B.D. (2007). Genome-wide analysis identifies a general requirement for polarity proteins in endocytic traffic. Nat Cell Biol *9*, 1066-1073.

Baum, B., and Perrimon, N. (2001). Spatial control of the actin cytoskeleton in Drosophila epithelial cells. Nat Cell Biol *3*, 883-890.

Behrens, J. (1999). Cadherins and catenins: role in signal transduction and tumor progression. Cancer metastasis reviews *18*, 15-30.

Blankenship, J.T., Fuller, M.T., and Zallen, J.A. (2007). The Drosophila homolog of the Exo84 exocyst subunit promotes apical epithelial identity. J Cell Sci *120*, 3099-3110.

Borghi, N., Sorokina, M., Shcherbakova, O.G., Weis, W.I., Pruitt, B.L., Nelson, W.J., and Dunn, A.R. (2012). E-cadherin is under constitutive actomyosin-generated tension that is increased at cell-cell contacts upon externally applied stretch. Proceedings of the National Academy of Sciences of the United States of America *109*, 12568-12573.

Bresnick, A.R. (1999). Molecular mechanisms of nonmuscle myosin-II regulation. Current opinion in cell biology *11*, 26-33.

Bryant, D.M., and Stow, J.L. (2004). The ins and outs of E-cadherin trafficking. Trends Cell Biol *14*, 427-434.

Canel, M., Serrels, A., Frame, M.C., and Brunton, V.G. (2013). E-cadherin-integrin crosstalk in cancer invasion and metastasis. Journal of cell science *126*, 393-401.

Canel, M., Serrels, A., Miller, D., Timpson, P., Serrels, B., Frame, M.C., and Brunton, V.G. (2010). Quantitative in vivo imaging of the effects of inhibiting integrin signaling via Src and FAK on cancer cell movement: effects on E-cadherin dynamics. Cancer Res *70*, 9413-9422.

Choquet, D., Felsenfeld, D.P., and Sheetz, M.P. (1997). Extracellular matrix rigidity causes strengthening of integrin-cytoskeleton linkages. Cell *88*, 39-48.

D'Souza-Schorey, C., and Chavrier, P. (2006). ARF proteins: roles in membrane traffic and beyond. Nat Rev Mol Cell Biol *7*, 347-358.

Danen, E.H., van Rheenen, J., Franken, W., Huveneers, S., Sonneveld, P., Jalink, K., and Sonnenberg, A. (2005). Integrins control motile strategy through a Rho-cofilin pathway. J Cell Biol *169*, 515-526.

de Rooij, J., Kerstens, A., Danuser, G., Schwartz, M.A., and Waterman-Storer, C.M. (2005). Integrin-dependent actomyosin contraction regulates epithelial cell scattering. The Journal of cell biology *171*, 153-164.

Debnath, J., Muthuswamy, S.K., and Brugge, J.S. (2003). Morphogenesis and oncogenesis of MCF-10A mammary epithelial acini grown in three-dimensional basement membrane cultures. Methods *30*, 256-268.

Dombrosky-Ferlan, P., Grishin, A., Botelho, R.J., Sampson, M., Wang, L., Rudert, W.A., Grinstein, S., and Corey, S.J. (2003). Felic (CIP4b), a novel binding partner with the Src kinase Lyn and Cdc42, localizes to the phagocytic cup. Blood *101*, 2804-2809.

Durer, U., Hartig, R., Bang, S., Thim, L., and Hoffmann, W. (2007). TFF3 and EGF induce different migration patterns of intestinal epithelial cells in vitro and trigger increased internalization of E-cadherin. Cellular physiology and biochemistry : international journal of experimental cellular physiology, biochemistry, and pharmacology *20*, 329-346.

Feng, Y., Hartig, S.M., Bechill, J.E., Blanchard, E.G., Caudell, E., and Corey, S.J. (2010). The Cdc42-interacting protein-4 (CIP4) gene knock-out mouse reveals delayed and decreased endocytosis. J Biol Chem *285*, 4348-4354.
Fricke, R., Gohl, C., Dharmalingam, E., Grevelhorster, A., Zahedi, B., Harden, N., Kessels, M., Qualmann, B., and Bogdan, S. (2009). Drosophila Cip4/Toca-1 integrates membrane trafficking and actin dynamics through WASP and SCAR/WAVE. Curr Biol *19*, 1429-1437.
Frost, A., Perera, R., Roux, A., Spasov, K., Destaing, O., Egelman, E.H., De Camilli, P., and Unger, V.M. (2008). Structural basis of membrane invagination by F-BAR domains. Cell *132*, 807-817.
Fujita, H., Katoh, H., Ishikawa, Y., Mori, K., and Negishi, M. (2002a). Rapostlin is a novel effector of Rnd2 GTPase inducing neurite branching. J Biol Chem *277*, 45428-45434.
Fujita, Y., Krause, G., Scheffner, M., Zechner, D., Leddy, H.E., Behrens, J., Sommer, T., and Birchmeier, W. (2002b). Hakai, a c-Cbl-like protein, ubiquitinates and induces endocytosis of the E-cadherin complex. Nat Cell Biol *4*, 222-231.
Gazdar, A.F., Kurvari, V., Virmani, A., Gollahon, L., Sakaguchi, M., Westerfield, M., Kodagoda, D., Stasny, V., Cunningham, H.T., Wistuba, II, *et al.* (1998). Characterization of paired tumor and non-tumor cell lines established from patients with breast cancer. International journal of cancer Journal international du cancer *78*, 766-774.
Georgiou, M., Marinari, E., Burden, J., and Baum, B. (2008). Cdc42, Par6, and aPKC regulate Arp2/3-mediated endocytosis to control local adherens junction stability. Curr Biol *18*, 1631-1638.
Giuliani, C., Troglio, F., Bai, Z., Patel, F.B., Zucconi, A., Malabarba, M.G., Disanza, A., Stradal, T.B., Cassata, G., Confalonieri, S., *et al.* (2009). Requirements for F-BAR proteins TOCA-1 and TOCA-2 in actin dynamics and membrane trafficking during Caenorhabditis elegans oocyte growth and embryonic epidermal morphogenesis. PLoS Genet *5*, e1000675.
Gumbiner, B.M. (2005). Regulation of cadherin-mediated adhesion in morphogenesis. Nat Rev Mol Cell Biol *6*, 622-634.
Halbleib, J.M., and Nelson, W.J. (2006). Cadherins in development: cell adhesion, sorting, and tissue morphogenesis. Genes Dev *20*, 3199-3214.
Harris, K.P., and Tepass, U. (2008). Cdc42 and Par proteins stabilize dynamic adherens junctions in the Drosophila neuroectoderm through regulation of apical endocytosis. J Cell Biol *183*, 1129-1143.
Ho, H.Y., Rohatgi, R., Lebensohn, A.M., Le, M., Li, J., Gygi, S.P., and Kirschner, M.W. (2004). Toca-1 mediates Cdc42-dependent actin nucleation by activating the N-WASP-WIP complex. Cell *118*, 203-216.
Hu, J., Mukhopadhyay, A., Truesdell, P., Chander, H., Mukhopadhyay, U.K., Mak, A.S., and Craig, A.W. (2011). Cdc42-interacting protein 4 is a Src substrate that regulates invadopodia and invasiveness of breast tumors by promoting MT1-MMP endocytosis. J Cell Sci *124*, 1739-1751.
Hu, M., Yao, J., Carroll, D.K., Weremowicz, S., Chen, H., Carrasco, D., Richardson, A., Violette, S., Nikolskaya, T., Nikolsky, Y., *et al.* (2008). Regulation of in situ to invasive breast carcinoma transition. Cancer cell *13*, 394-406.
Itoh, T., Erdmann, K.S., Roux, A., Habermann, B., Werner, H., and De Camilli, P. (2005). Dynamin and the actin cytoskeleton cooperatively regulate plasma membrane invagination by BAR and F-BAR proteins. Dev Cell *9*, 791-804.
Janda, E., Nevolo, M., Lehmann, K., Downward, J., Beug, H., and Grieco, M. (2006). Raf plus TGFbeta-dependent EMT is initiated by endocytosis and lysosomal degradation of E-cadherin. Oncogene *25*, 7117-7130.
Kardash, E., Bandemer, J., and Raz, E. (2011). Imaging protein activity in live embryos using fluorescence resonance energy transfer biosensors. Nat Protoc *6*, 1835-1846.
Kim, S.H., Li, Z., and Sacks, D.B. (2000). E-cadherin-mediated cell-cell attachment activates Cdc42. J Biol Chem *275*, 36999-37005.
Langevin, J., Morgan, M.J., Sibarita, J.B., Aresta, S., Murthy, M., Schwarz, T., Camonis, J., and Bellaiche, Y. (2005). Drosophila exocyst components Sec5, Sec6, and Sec15 regulate DE-Cadherin trafficking from recycling endosomes to the plasma membrane. Dev Cell *9*, 365-376.

le Duc, Q., Shi, Q., Blonk, I., Sonnenberg, A., Wang, N., Leckband, D., and de Rooij, J. (2010). Vinculin potentiates E-cadherin mechanosensing and is recruited to actin-anchored sites within adherens junctions in a myosin II-dependent manner. The Journal of cell biology *189*, 1107-1115.

Le, T.L., Yap, A.S., and Stow, J.L. (1999). Recycling of E-cadherin: a potential mechanism for regulating cadherin dynamics. J Cell Biol *146*, 219-232.

Leibfried, A., Fricke, R., Morgan, M.J., Bogdan, S., and Bellaiche, Y. (2008). Drosophila Cip4 and WASp Define a Branch of the Cdc42-Par6-aPKC Pathway Regulating E-Cadherin Endocytosis. Curr Biol *18*, 1639-1648.

Levayer, R., Pelissier-Monier, A., and Lecuit, T. (2011). Spatial regulation of Dia and Myosin-II by RhoGEF2 controls initiation of E-cadherin endocytosis during epithelial morphogenesis. Nat Cell Biol.

Linder, S., Hufner, K., Wintergerst, U., and Aepfelbacher, M. (2000). Microtubule-dependent formation of podosomal adhesion structures in primary human macrophages. J Cell Sci *113 Pt 23*, 4165-4176.

Lock, P., Abram, C.L., Gibson, T., and Courtneidge, S.A. (1998). A new method for isolating tyrosine kinase substrates used to identify fish, an SH3 and PX domain-containing protein, and Src substrate. The EMBO journal *17*, 4346-4357.

Lodhi, I.J., Chiang, S.H., Chang, L., Vollenweider, D., Watson, R.T., Inoue, M., Pessin, J.E., and Saltiel, A.R. (2007). Gapex-5, a Rab31 guanine nucleotide exchange factor that regulates Glut4 trafficking in adipocytes. Cell metabolism *5*, 59-72.

Lozano, E., Betson, M., and Braga, V.M. (2003). Tumor progression: Small GTPases and loss of cell-cell adhesion. Bioessays *25*, 452-463.

Malet-Engra, G., Viaud, J., Ysebaert, L., Farce, M., Lafouresse, F., Laurent, G., Gaits-Iacovoni, F., Scita, G., and Dupre, L. (2013). CIP4 controls CCL19-driven cell steering and chemotaxis in chronic lymphocytic leukemia. Cancer research.

Miller, F.R., Santner, S.J., Tait, L., and Dawson, P.J. (2000). MCF10DCIS.com xenograft model of human comedo ductal carcinoma in situ. Journal of the National Cancer Institute *92*, 1185-1186.

Miller, J.R., and McClay, D.R. (1997). Characterization of the role of cadherin in regulating cell adhesion during sea urchin development. Dev Biol *192*, 323-339.

Muthuswamy, S.K., Li, D., Lelievre, S., Bissell, M.J., and Brugge, J.S. (2001). ErbB2, but not ErbB1, reinitiates proliferation and induces luminal repopulation in epithelial acini. Nat Cell Biol *3*, 785-792.

Ogata, S., Morokuma, J., Hayata, T., Kolle, G., Niehrs, C., Ueno, N., and Cho, K.W. (2007). TGF-beta signaling-mediated morphogenesis: modulation of cell adhesion via cadherin endocytosis. Genes Dev *21*, 1817-1831.

Orlichenko, L., Weller, S.G., Cao, H., Krueger, E.W., Awoniyi, M., Beznoussenko, G., Buccione, R., and McNiven, M.A. (2009). Caveolae mediate growth factor-induced disassembly of adherens junctions to support tumor cell dissociation. Mol Biol Cell *20*, 4140-4152.

Palacios, F., Tushir, J.S., Fujita, Y., and D'Souza-Schorey, C. (2005). Lysosomal targeting of E-cadherin: a unique mechanism for the down-regulation of cell-cell adhesion during epithelial to mesenchymal transitions. Molecular and cellular biology *25*, 389-402.

Paterson, A.D., Parton, R.G., Ferguson, C., Stow, J.L., and Yap, A.S. (2003). Characterization of E-cadherin endocytosis in isolated MCF-7 and chinese hamster ovary cells: the initial fate of unbound E-cadherin. J Biol Chem *278*, 21050-21057.

Peinado, H., Portillo, F., and Cano, A. (2004). Transcriptional regulation of cadherins during development and carcinogenesis. The International journal of developmental biology *48*, 365-375.

Petersen, O.W., Ronnov-Jessen, L., Howlett, A.R., and Bissell, M.J. (1992). Interaction with basement membrane serves to rapidly distinguish growth and differentiation pattern of normal and malignant human breast epithelial cells. Proceedings of the National Academy of Sciences of the United States of America *89*, 9064-9068.

Pichot, C.S., Arvanitis, C., Hartig, S.M., Jensen, S.A., Bechill, J., Marzouk, S., Yu, J., Frost, J.A., and Corey, S.J. (2010). Cdc42-interacting protein 4 promotes breast cancer cell invasion and formation of invadopodia through activation of N-WASp. Cancer Res *70*, 8347-8356.
Qian, X., Karpova, T., Sheppard, A.M., McNally, J., and Lowy, D.R. (2004). E-cadherin-mediated adhesion inhibits ligand-dependent activation of diverse receptor tyrosine kinases. EMBO J *23*, 1739-1748.
Ren, X.D., Kiosses, W.B., and Schwartz, M.A. (1999). Regulation of the small GTP-binding protein Rho by cell adhesion and the cytoskeleton. The EMBO journal *18*, 578-585.
Reshetnikova, G., Troyanovsky, S., and Rimm, D.L. (2007). Definition of a direct extracellular interaction between Met and E-cadherin. Cell biology international *31*, 366-373.
Reynolds, A.B., and Roczniak-Ferguson, A. (2004). Emerging roles for p120-catenin in cell adhesion and cancer. Oncogene *23*, 7947-7956.
Roberts, M., Barry, S., Woods, A., van der Sluijs, P., and Norman, J. (2001). PDGF-regulated rab4-dependent recycling of alphavbeta3 integrin from early endosomes is necessary for cell adhesion and spreading. Curr Biol *11*, 1392-1402.
Saengsawang, W., Mitok, K., Viesselmann, C., Pietila, L., Lumbard, D.C., Corey, S.J., and Dent, E.W. (2012). The F-BAR protein CIP4 inhibits neurite formation by producing lamellipodial protrusions. Current biology : CB *22*, 494-501.
Seton-Rogers, S.E., Lu, Y., Hines, L.M., Koundinya, M., LaBaer, J., Muthuswamy, S.K., and Brugge, J.S. (2004). Cooperation of the ErbB2 receptor and transforming growth factor beta in induction of migration and invasion in mammary epithelial cells. Proceedings of the National Academy of Sciences of the United States of America *101*, 1257-1262.
Shaye, D.D., Casanova, J., and Llimargas, M. (2008). Modulation of intracellular trafficking regulates cell intercalation in the Drosophila trachea. Nat Cell Biol *10*, 964-970.
Shen, Y., Hirsch, D.S., Sasiela, C.A., and Wu, W.J. (2008). Cdc42 regulates E-cadherin ubiquitination and degradation through an epidermal growth factor receptor to Src-mediated pathway. J Biol Chem *283*, 5127-5137.
Singh, R., Lei, P., and Andreadis, S.T. (2009). PKC-delta binds to E-cadherin and mediates EGF-induced cell scattering. Experimental cell research *315*, 2899-2913.
Sorkin, A., and Duex, J.E. (2010). Quantitative analysis of endocytosis and turnover of epidermal growth factor (EGF) and EGF receptor. Curr Protoc Cell Biol *Chapter 15*, Unit 15 14.
Taylor, M.J., Perrais, D., and Merrifield, C.J. (2011). A high precision survey of the molecular dynamics of mammalian clathrin-mediated endocytosis. PLoS Biol *9*, e1000604.
Thiery, J.P., Acloque, H., Huang, R.Y., and Nieto, M.A. (2009). Epithelial-mesenchymal transitions in development and disease. Cell *139*, 871-890.
Tian, L., Nelson, D.L., and Stewart, D.M. (2000). Cdc42-interacting protein 4 mediates binding of the Wiskott-Aldrich syndrome protein to microtubules. J Biol Chem *275*, 7854-7861.
Torres, E., and Rosen, M.K. (2003). Contingent phosphorylation/dephosphorylation provides a mechanism of molecular memory in WASP. Mol Cell *11*, 1215-1227.
Wakita, Y., Kakimoto, T., Katoh, H., and Negishi, M. (2011). The F-BAR protein Rapostlin regulates dendritic spine formation in hippocampal neurons. The Journal of biological chemistry *286*, 32672-32683.
Wang, Y., Cao, H., Chen, J., and McNiven, M.A. (2011). A Direct Interaction Between the Large GTPase Dynamin2 and FAK Regulate Focal Adhesion Dynamics in Response to Active Src. Mol Biol Cell.
Wu, M., Huang, B., Graham, M., Raimondi, A., Heuser, J.E., Zhuang, X., and De Camilli, P. (2010). Coupling between clathrin-dependent endocytic budding and F-BAR-dependent tubulation in a cell-free system. Nat Cell Biol *12*, 902-908.
Zheng, G., Lyons, J.G., Tan, T.K., Wang, Y., Hsu, T.T., Min, D., Succar, L., Rangan, G.K., Hu, M., Henderson, B.R., *et al.* (2009). Disruption of E-cadherin by matrix metalloproteinase directly mediates epithelial-mesenchymal transition downstream of transforming growth factor-beta1 in renal tubular epithelial cells. Am J Pathol *175*, 580-591.

Zhurinsky, J., Shtutman, M., and Ben-Ze'ev, A. (2000). Differential mechanisms of LEF/TCF family-dependent transcriptional activation by beta-catenin and plakoglobin. Molecular and cellular biology *20*, 4238-4252.

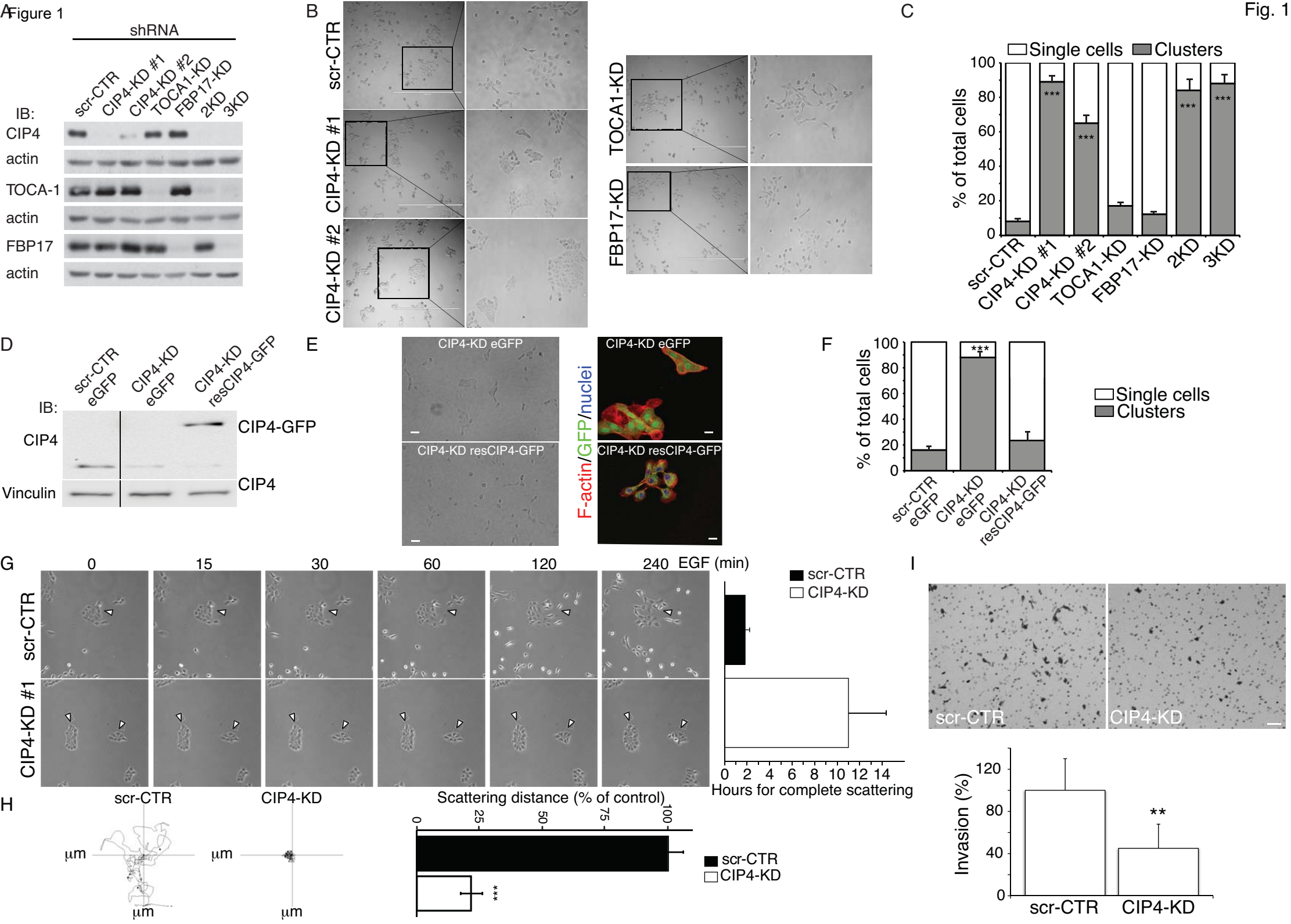
A
shRNA
scr-CTR
CIP4-KD #1
CIP4-KD #2
TOCA1-KD
FBP17-KD
2KD
3KD
IB:
CIP4
actin
TOCA-1
actin
FBP17
actin
B
scr-CTR
CIP4-KD #1
CIP4-KD #2
TOCA1-KD
FBP17-KD
C
Single cells
Clusters
% of total cells
100
80
60
40
20
0
***
scr-CTR
CIP4-KD #1
CIP4-KD #2
TOCA1-KD
FBP17-KD
2KD
3KD
D
scr-CTR eGFP
CIP4-KD eGFP
CIP4-KD resCIP4-GFP
IB:
CIP4
CIP4-GFP
Vinculin
CIP4
E
CIP4-KD eGFP
CIP4-KD resCIP4-GFP
F-actin/GFP/nuclei
F
% of total cells
Single cells
Clusters
scr-CTR eGFP
CIP4-KD eGFP
CIP4-KD resCIP4-GFP
G
0
15
30
60
120
240
EGF (min)
scr-CTR
CIP4-KD #1
scr-CTR
CIP4-KD
Hours for complete scattering
H
scr-CTR
CIP4-KD
μm
Scattering distance (% of control)
scr-CTR
CIP4-KD
I
scr-CTR
CIP4-KD
Invasion (%)
scr-CTR
CIP4-KD

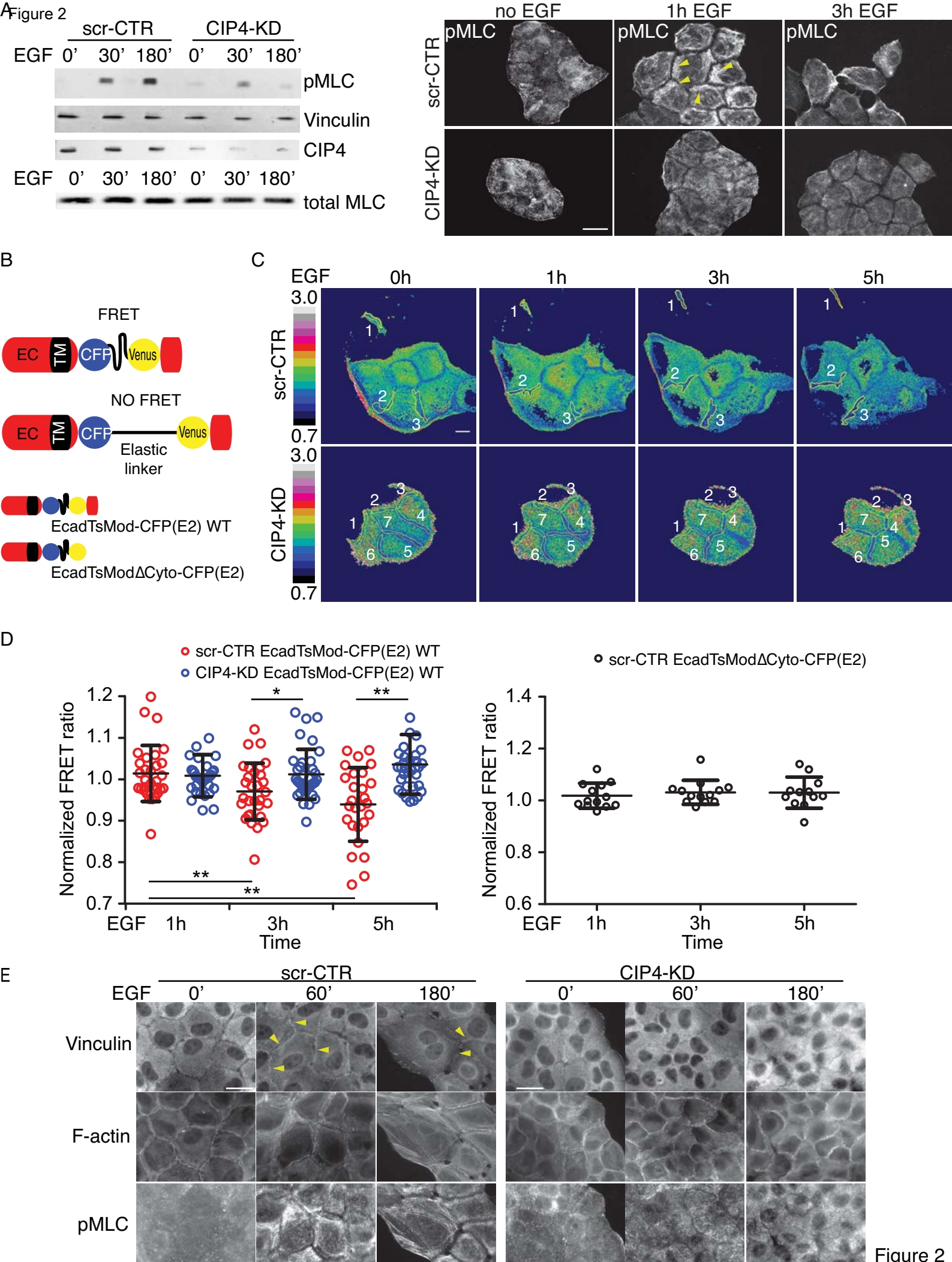
A
scr-CTR
CIP4-KD
EGF 0' 30' 180' 0' 30' 180'
pMLC
Vinculin
CIP4
EGF 0' 30' 180' 0' 30' 180'
total MLC
no EGF
1h EGF
3h EGF
scr-CTR
CIP4-KD
pMLC
B
FRET
EC
TM
CFP
Venus
NO FRET
Elastic linker
EcadTsMod-CFP(E2) WT
EcadTsModΔCyto-CFP(E2)
C
EGF
0h
1h
3h
5h
3.0
0.7
scr-CTR
CIP4-KD
D
scr-CTR EcadTsMod-CFP(E2) WT
CIP4-KD EcadTsMod-CFP(E2) WT
Normalized FRET ratio
1.2
1.1
1.0
0.9
0.8
0.7
*
**
**
**
EGF 1h 3h 5h
Time
scr-CTR EcadTsModΔCyto-CFP(E2)
Normalized FRET ratio
1.4
1.2
1.0
0.8
0.6
EGF 1h 3h 5h
Time
E
scr-CTR
CIP4-KD
EGF 0' 60' 180' 0' 60' 180'
Vinculin
F-actin
pMLC

Figure 2

Figure 3

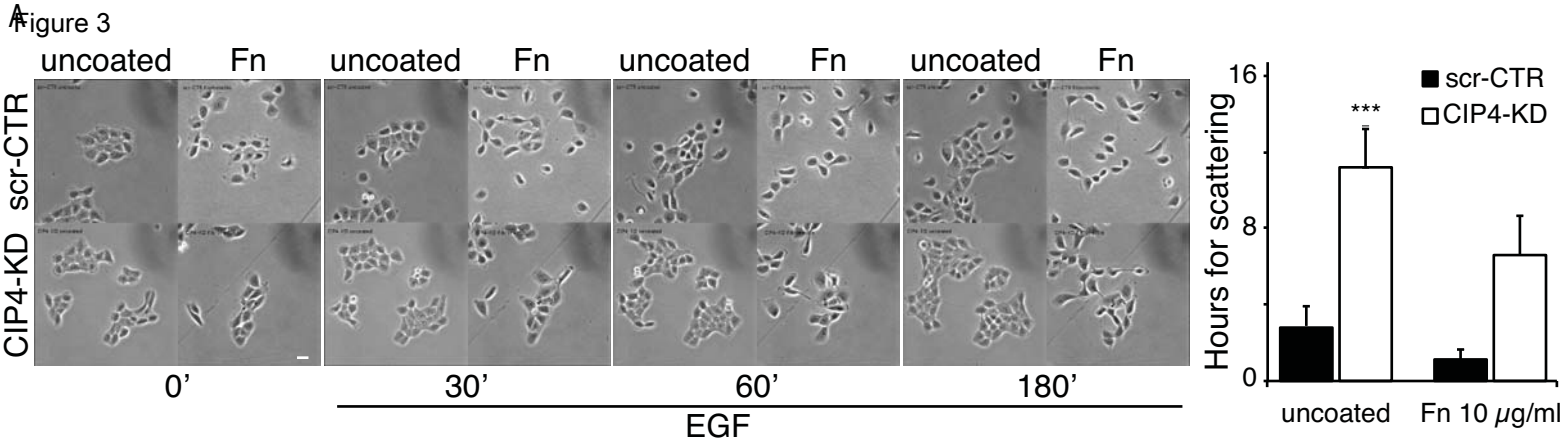

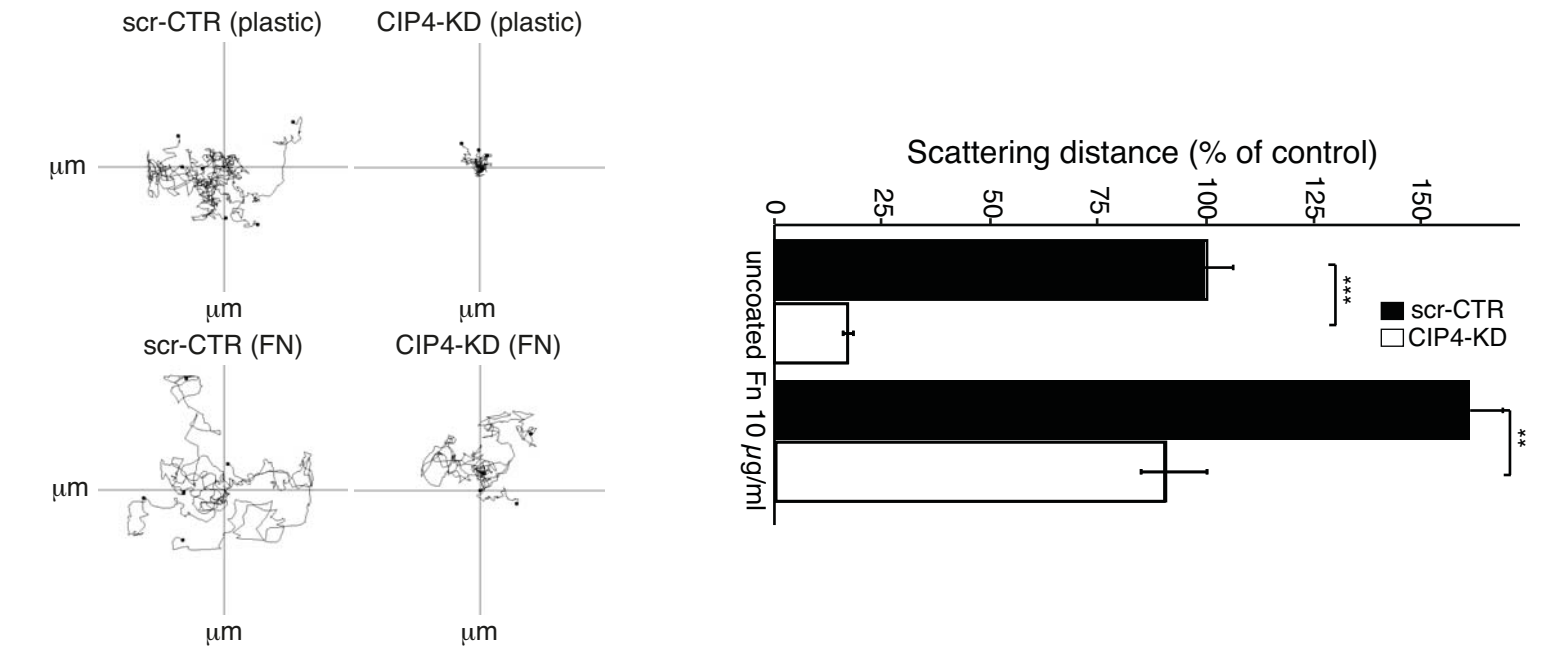

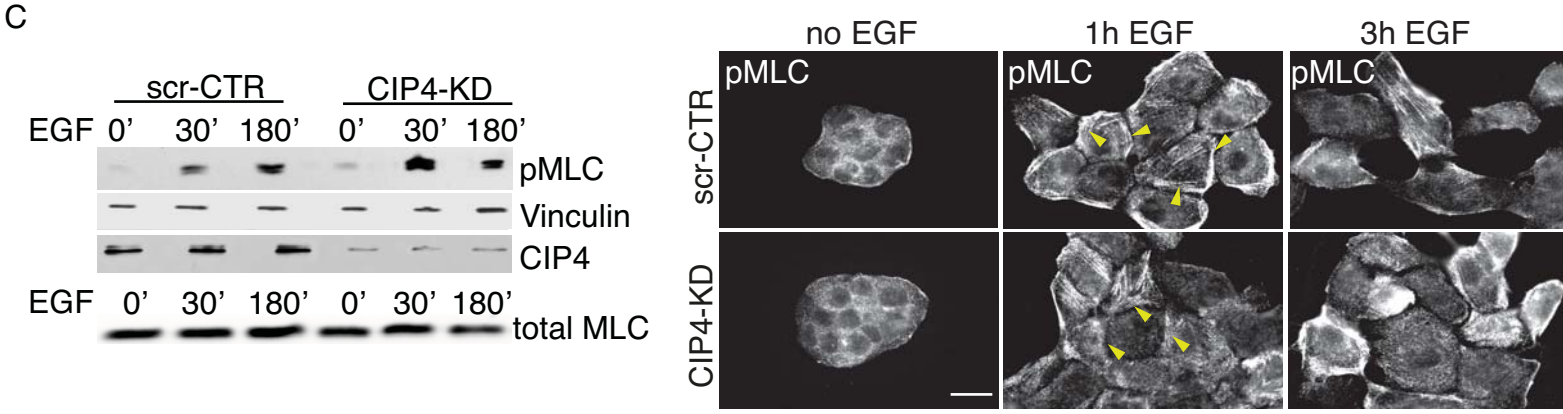

Fig. 3

A

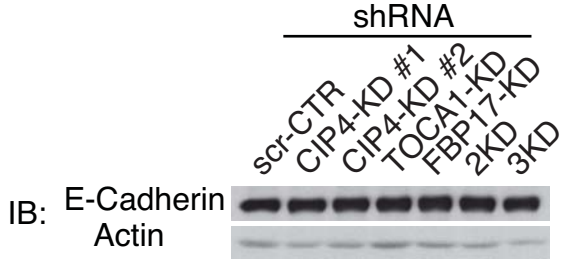
shRNA
scr-CTR
CIP4-KD #1
CIP4-KD #2
TOCA1-KD
FBP17-KD
2KD
3KD
IB: E-Cadherin
Actin

B

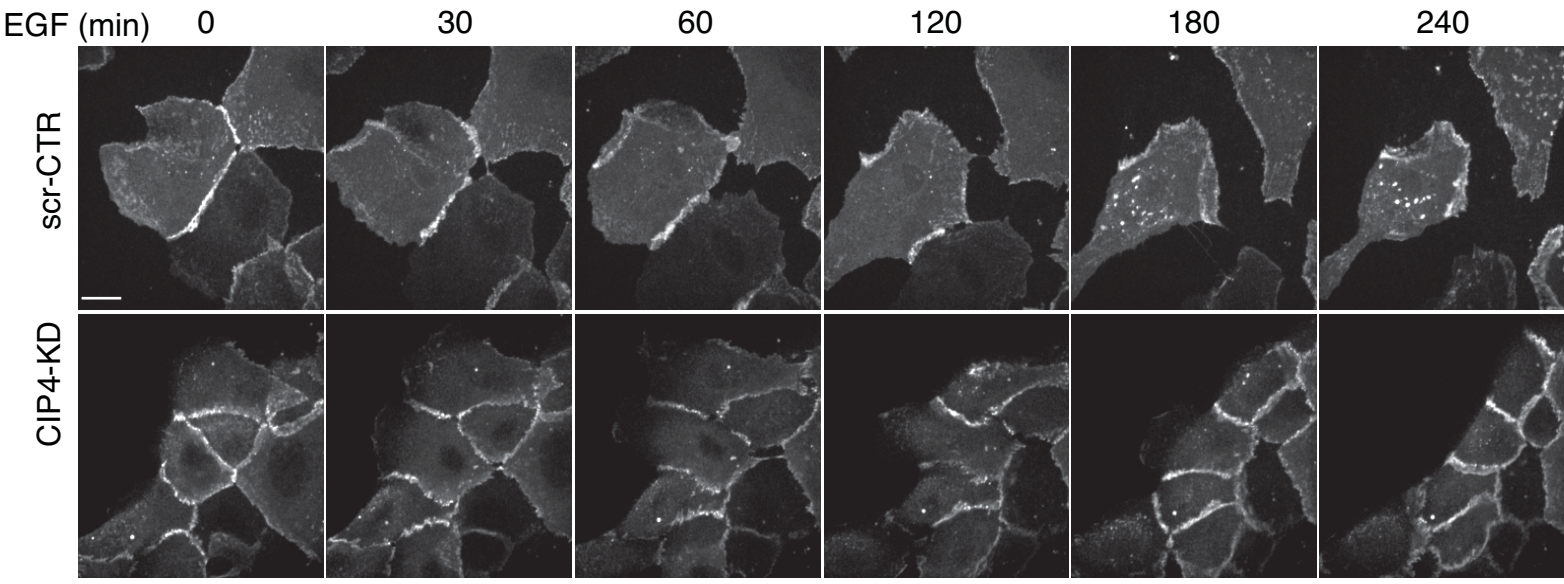
EGF (min)
0
30
60
120
180
240
scr-CTR
CIP4-KD

C

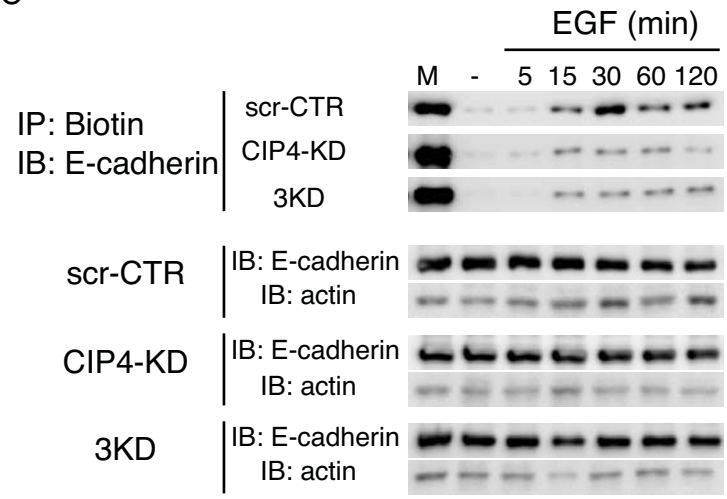
EGF (min)
M
-
5
15
30
60
120
IP: Biotin
IB: E-cadherin
scr-CTR
CIP4-KD
3KD
IB: E-cadherin
IB: actin

D

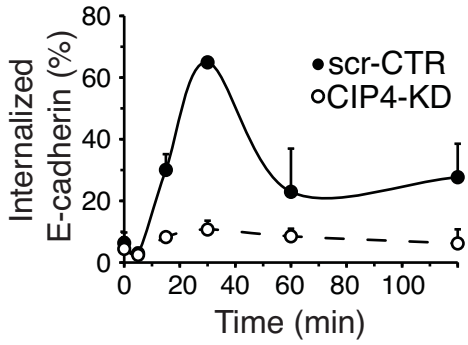
Internalized E-cadherin (%)
scr-CTR
CIP4-KD
Time (min)

E

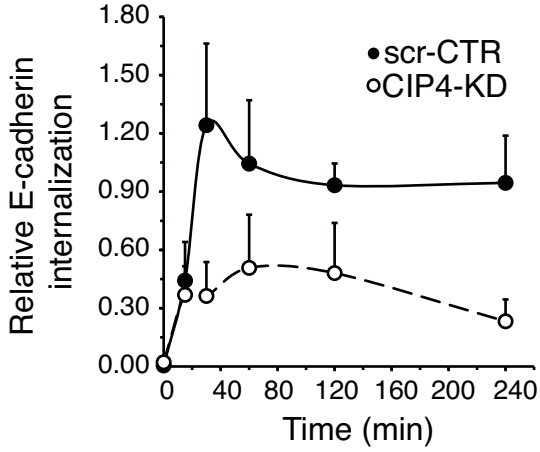
Relative E-cadherin internalization
scr-CTR
CIP4-KD
Time (min)

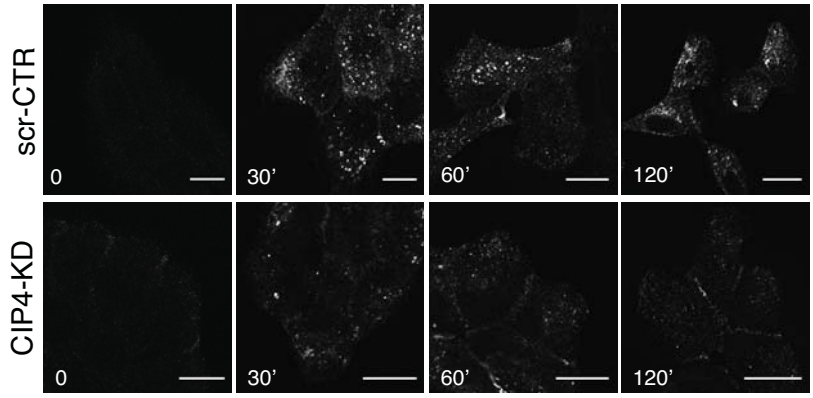
scr-CTR
CIP4-KD
0
30'
60'
120'

Fig. 4

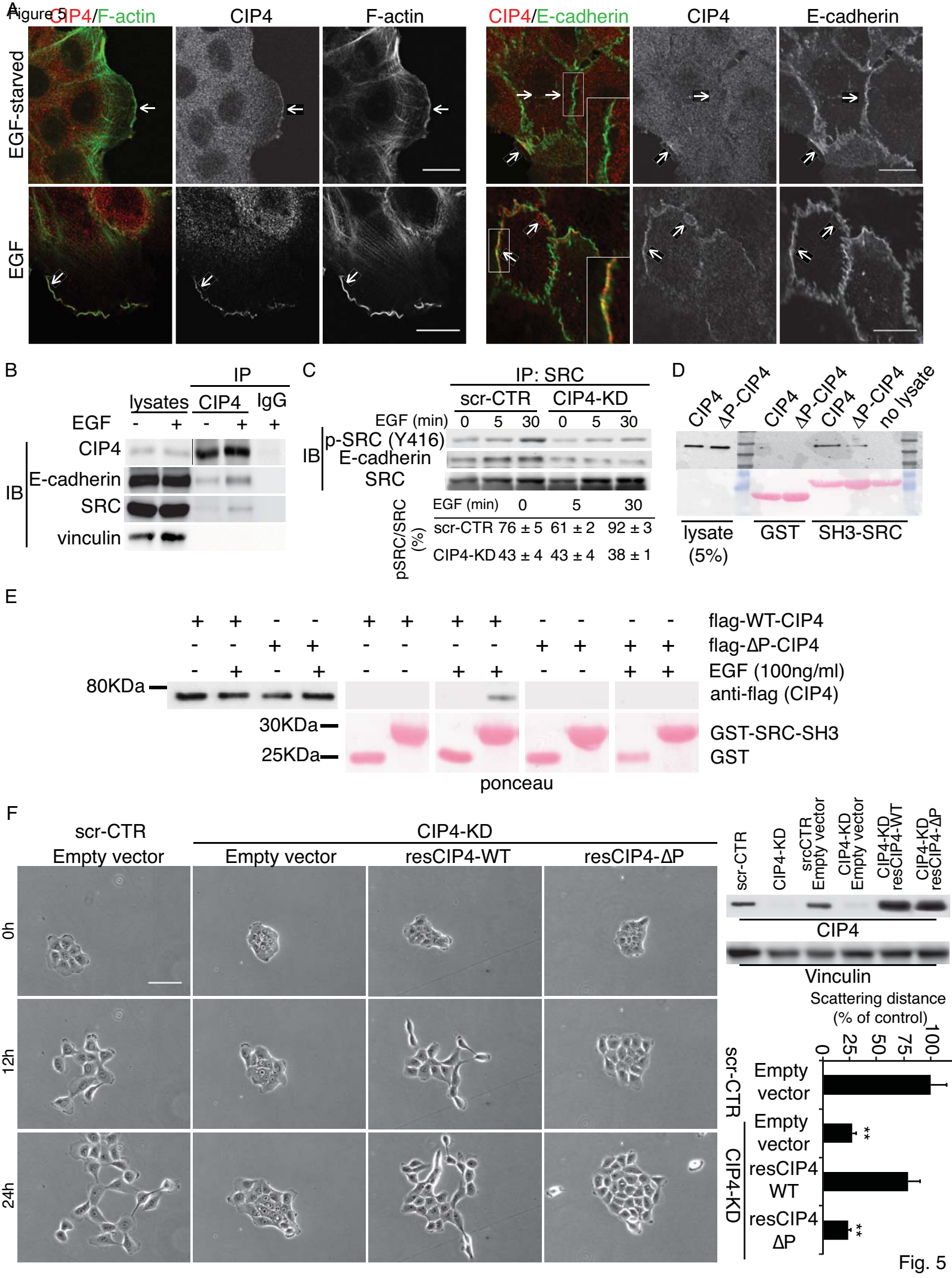

Figure 5

Fig. 5

Figure 6

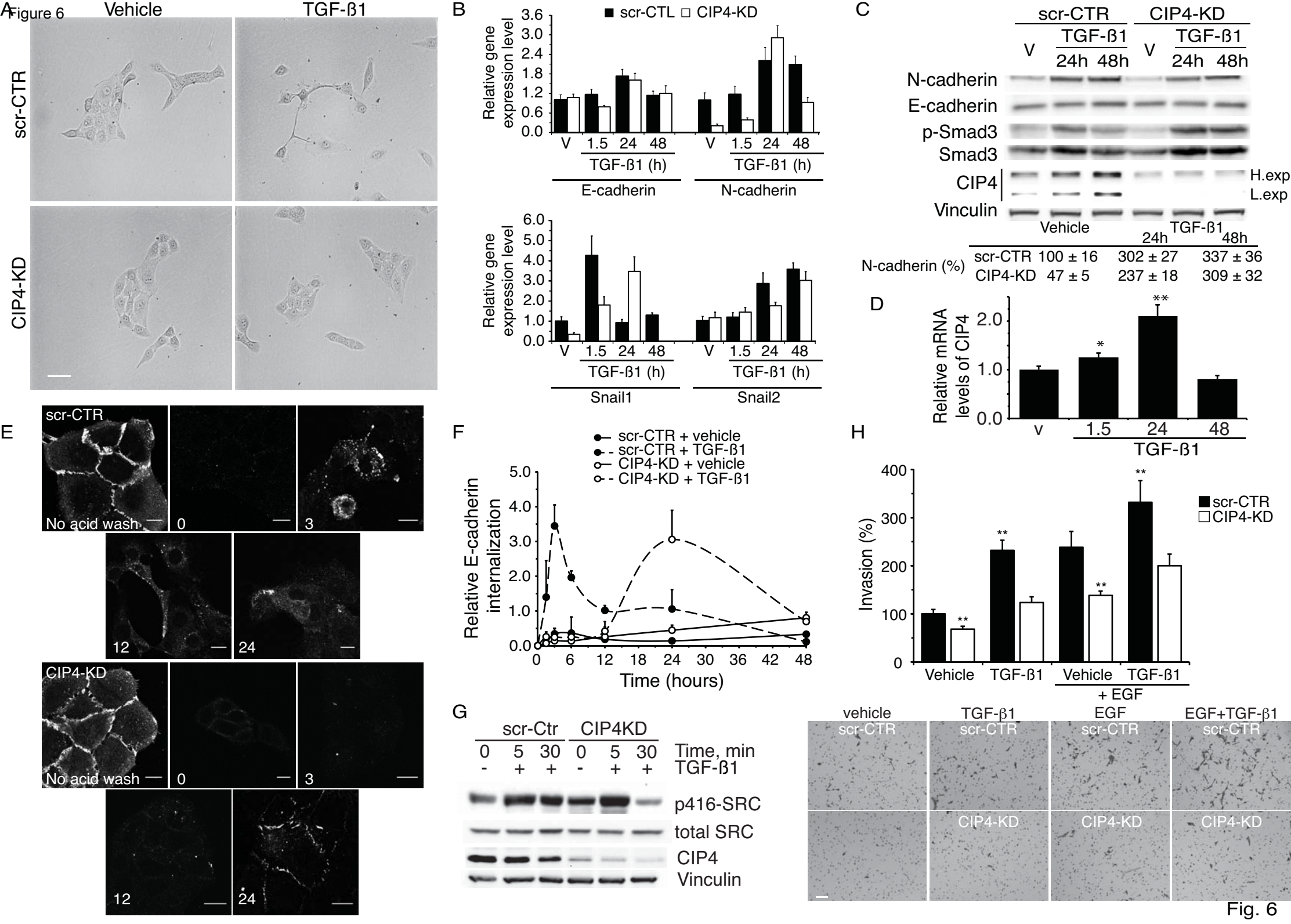

Fig. 6

Figure 7

A

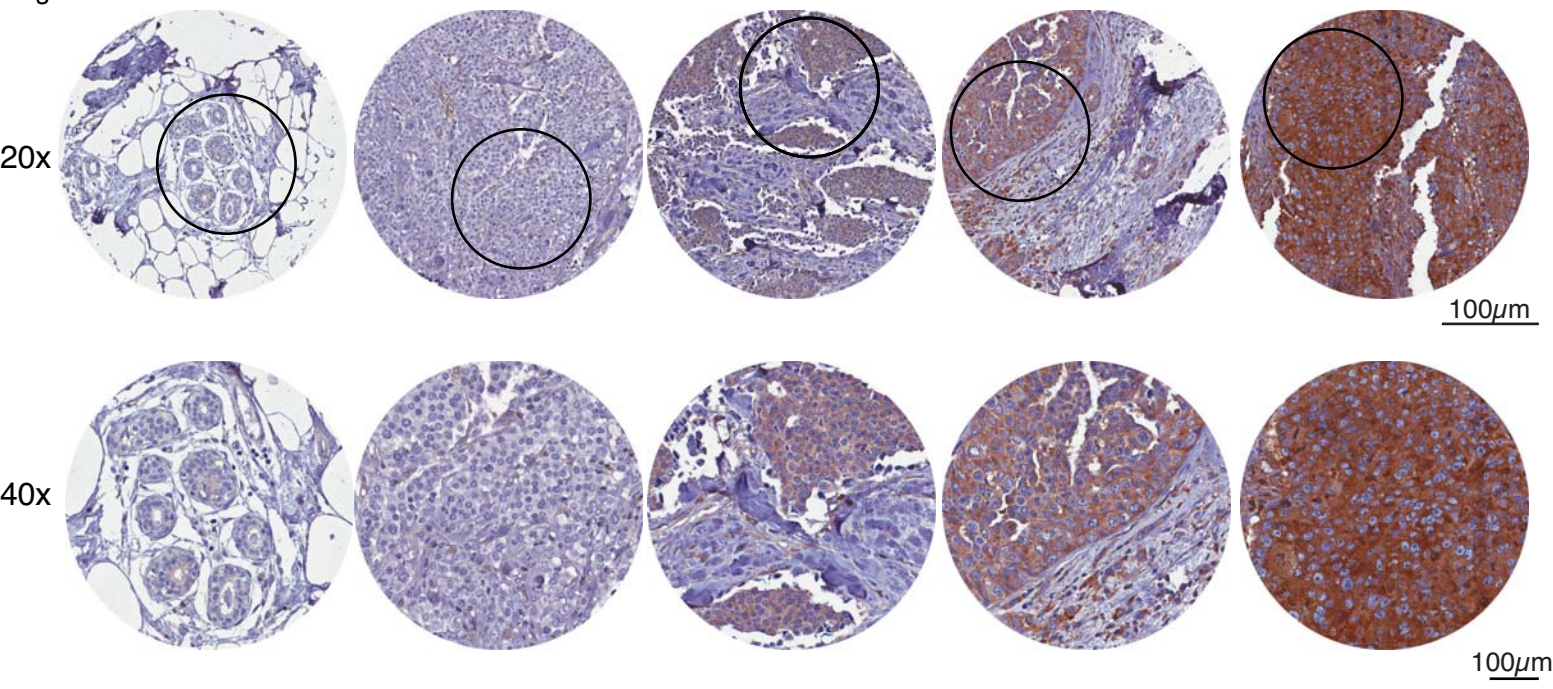

B

		CIP4 LOW	CIP4 HIGH	χ2 P-value
All Patients		262	51 (16.29 %)	
ER	NEG	68	28 (**29.17 %**)	
	POS	187	22 (10.53 %)	**>0.001**
PgR	NEG	96	31 (**24.41 %**)	
	POS	159	19 (10.57 %)	**0.0014**
Ki67	NEG	88	13 (12.87 %)	
	POS	167	37 (18.14 %)	0.242
ErbB2	NEG	225	36 (13.79 %)	
	POS	22	10 (**31.25 %**)	**0.0104**
pT	1	139	23 (14.20 %)	
	2-3-4	123	27 (18%)	0.36
GRADE	G1	43	7 (14 %)	
	G2	103	16 (13.45 %)	
	G3	88	20 (18.52 %)	0.548
Node	NEG	112	150 (57.25 %)	
	POS	24	27 (52.99 %)	0.569
NPI	GPG	65	9 (12.16 %)	
	MPG	69	23 (18.85 %)	
	PPG	67	11 (14.10 %)	0.413
Any Event	NO	133	15 (10.14 %)	
	YES	129	36 (**21.82 %**)	**0.0046**
Distant Relapse	NO	189	32 (14.48 %)	
	YES	73	19 (20.65 %)	0.178
Status	Alive	186	30 (14.29 %)	
	Dead	82	21 (20.39 %)	0.169

C

ErbB2 Negative Tumors		**CIP4 LOW**	**CIP4 HIGH**	**χ2 P-value**
Any Event	NO	122	13 (9.63 %)	
	YES	129	23 (**18.25 %**)	**0.0426**
ER Positive Tumors		**CIP4 LOW**	**CIP4 HIGH**	**χ2 P-value**
Any Event	NO	97	6 (2.87 %)	
	YES	90	16 (**7.66 %**)	**0.0263**
PgR Positive Tumors		**CIP4 LOW**	**CIP4 HIGH**	**χ2 P-value**
Any Event	NO	91	6 (3.37 %)	
	YES	68	13 (**7.30 %**)	**0.0331**
G2 Tumors		**CIP4 LOW**	**CIP4 HIGH**	**χ2 P-value**
Any Event	NO	59	4 (3.36 %)	
	YES	44	12 (**10.08 %**)	**0.0146**

D

No Event versus Any Event (Univariate)

Level1	**/Level2**	**Odds Ratio**	**Lower 95%**	**Upper 95%**	**P value**
CIP4 LOW	CIP4 HIGH	2.474	1.316	4.860	***0.0046***

No Event versus Any Event (Multivariate)

Level1	**/Level2**	**Odds Ratio**	**Lower 95%**	**Upper 95%**	**P value**
CIP4 LOW	CIP4 HIGH	2.413	1.007	6.021	***0.0482***
Ductal	Lobular	1.372	0.576	3.300	0.4739
pT1	pT2-3-4	2.310	1.279	4.194	***0.0056***
Node NEG	Node POS	3.874	2.145	7.139	***<0001***
G1-G2	G3	2.188	1.123	4.313	***0.0214***
ER NEG	ER POS	2.164	0.973	4.986	0.0584
PgR NEG	PgR POS	0.572	0.264	1.219	0.1481
Ki 67 LOW	Ki67 HIGH	1.279	0.645	2.538	0.4797
ErbB2 NEG	ErbB2 POS	2.590	0.920	7.903	0.072

Fig. 7

Figure 8

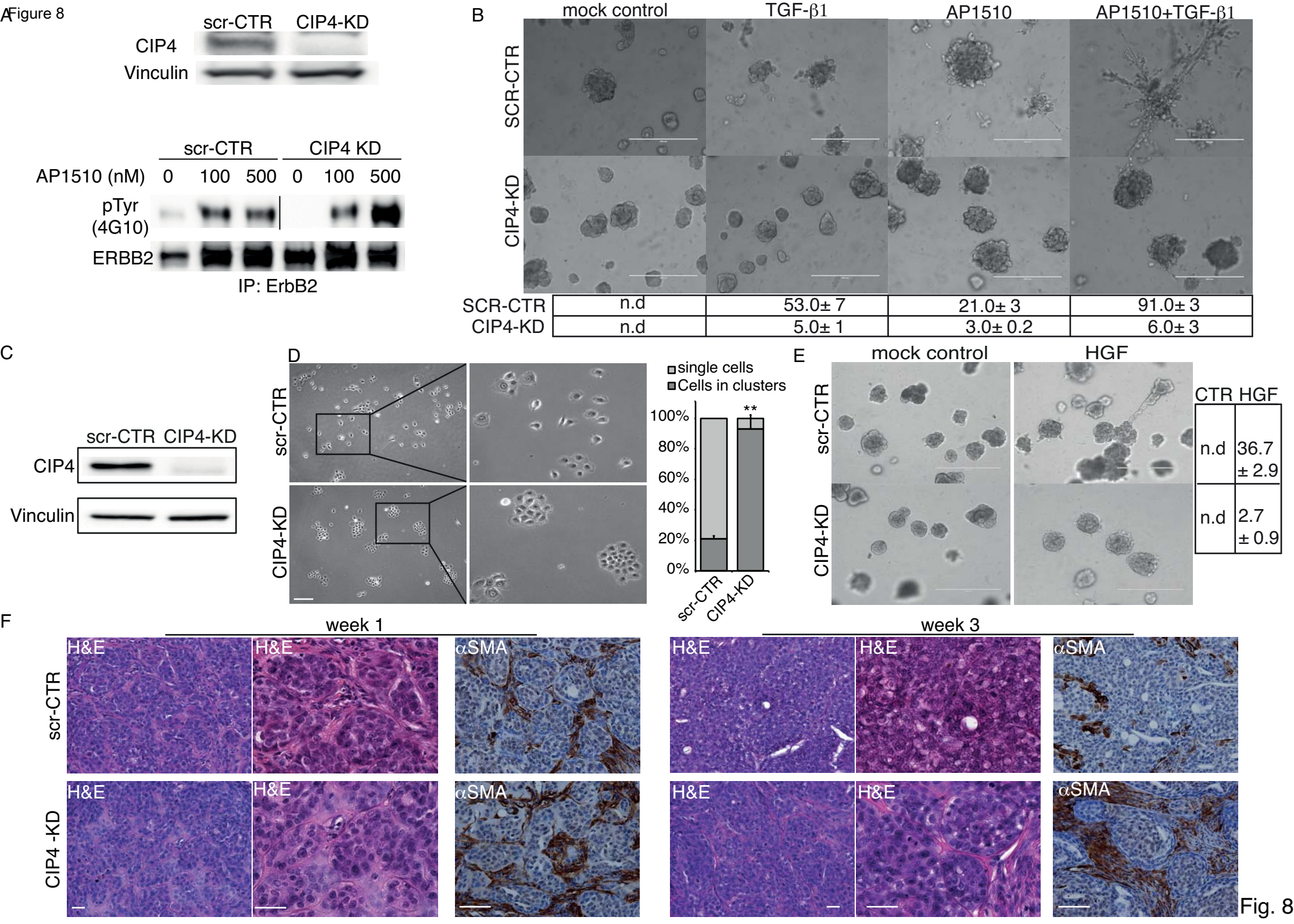

Fig. 8

Inventory of Supplementary Materials

Supplemental Figure Legends

Supplemental Movie legends

Supplementary Experimental Procedures

References

SUPPLEMENTAL INFORMATION

Supplemental Figure Legends

Figure S1: Expression of CIP4 regulates MCF10A cell compaction. (related to Figure 1)

(**A**) MCF10A cells were infected with lentiviruses expressing scramble control shRNA (scr-CTR) or shRNAs against TOCA family proteins, individually (CIP-KD #1/#2; TOCA1-KD; FBP17-KD) or in combination (CIP4/TOCA-1 double KD - 2KD; CIP4/TOCA-1/FBP17 triple KD - 3KD). Representative phase contrast images of the indicated cells grown in complete medium are shown. Bar, 150 µm.

(**B**) MCF10A cells devoid of TOCA family members and grown in complete medium, were fixed and stained to detect E-cadherin (green), F-actin (red) and nuclei (blue). Right panels show magnifications of boxed areas.

(**C**) Quantification of junctional E-cadherin. The intensity of randomly chosen areas of junctional E-cadherin in the confocal images shown in (**B)** was normalized with respect to cytoplasmic areas of identical size and expressed as a ratio. Data are the mean±s.e.m (n=5).

(**D**) MTT proliferation assay was performed for the different MCF10A sublines grown in complete medium. Data are expressed as % of scr-CTR cells.

(**E**) Scr-CTR and CIP4-KD MCF10A cells grown in the presence of complete medium were fixed and stained for giantin (red), F-actin (green) and nuclei (blue). Arrows indicate examples of cells with outwardly polarized distribution of the Golgi apparatus. Bottom images are magnification of the boxed areas. Bottom graph, the percentage of cells displaying Golgi oriented toward the outside of the cluster with respect to the nucleus was quantified in three independent experiments counting > 100 cells/experiment.

(**F**) Representative confocal images showing basolateral F-actin staining in the different MCF10A sublines. Insets show a higher magnification of selected areas. Bar, 20 µm. (**P*<0.05 and ****P*<0.001 compared to scr-CTR MCF10A cells determined by the paired Student's t-test).

Figure S2: CIP4 expression modulates the motility of clustered MCF10A cells, without affecting the parameter of individual cell migration. (Related to Figure 1)

(***A)*** Migration of randomly chosen control (scr-CTR) or MCF10A cells devoid of TOCA family members was monitored in complete medium containing EGF, by time-lapse microscopy (Movie S1A and B). Graphs represent tracks of cells moving over a 24-hour period (a minimum of 50 cells were analyzed for each cell genotype). CIP4-KD cells stop migrating once entering contacting a cluster. Whereas control cells that have come into contact with each other or a cluster frequently detach and resume their motility.

(**B**) Cell locomotion was by analyzed subdividing cells undergoing two distinct mode of motility: 1) the "single motility mode" during which cells move without touching each other or a cluster and 2) the "cluster motility mode" during which cells come into contact with each other or with a cluster. During single motility mode, cells move at a speed that is independent from the removal of CIP4. Conversely, silencing of CIP4 decreases significantly the motility of the cells coming into contact with cluster

since they can no longer detach from it and ceased migration. ** P<0.001 compared to scr-CTR MCF10A cells based on the paired Student's t-test; n.s. not significant.
(**C**) Wound healing assay performed with scr-CTR and CIP4-KD#1 MCF10A cells. Representative phase contract images at the indicated time points are shown. Scale Bar,100 μm. Wound closure was quantified by measuring the wound area at different time points. Data are expressed as the % of wound area at the indicated time with respect to time 0.
(**D**) Scr-CTR and CIP4-KD #1 MCF10A cells cultured in complete or EGF-depleted medium were imaged by phase-contrast microscopy. Bar, 400 μm.
(**E**) Immunofluorescence staining to detect F-actin (red), E-cadherin (green) and nuclei (blue) of EGF-deprived control (scr-CTR) or the indicated TOCA family-KD MCF10A cells. Magnifications of boxed areas are shown on the right. Bar, 20 μm.

Figure S3: EGFR internalization, activation and downstream signaling are not affected by CIP4 depletion.
(**A**) Total cell lysates of control (scr-CTR) or MCF10A cells devoid of TOCA family proteins grown sparsely or confluent were IB with the indicated antibodies.
(**B**) Cell surface levels of EGFR were quantified in the MCF10A cell sub-lines as described in Suppl. Experimental Procedure. The number of cell surface receptors was deduced from the specific activities of ^{125}I-EGF.
(**C**) EGFR degradation and activation of MAPK/ERK pathway was assessed in control or CIP4-KD #1 MCF10A cells after acute EGF stimulation (100 ng/ml) by immunoblotting (IB) with the indicated antibodies. Vinculin was used as a loading control. The relative intensity of the pAKT and pERK1/2 signals with respect to total AKT and ERK1/2 was quantified by densitometry analysis.
(**D**) Internalization of ^{125}I-EGF was studied in scr-CTR and CIP4-KD MCF10A cells as described in Experimental Procedures. The rate of internalization is expressed as the ratio between internalized and surface ^{125}I-EGF for each time point.
(**E**) Recycling of EGFR was determined in scr-CTR and CIP4-KD #1 MCF10A cells by measuring surface-bound and intracellular ^{125}I-EGF levels. For each time point, the medium was collected and subjected to TCA precipitation to determine the amount of intact ^{125}I-EGF. Data are expressed as the percentage of intact internalized ^{125}I-EGF in the medium with respect to the total ^{125}I-EGF.
(**F**) scr-CTR and CIP4-KD #1 MCF10A cells were stimulated with EGF (100 ng/ml) for the indicated times. Phosphorylated (Tyr1068; pEGFR) and total EGFR were then assessed in total cell lysates by IB with the indicated antibodies. The relative intensity of the pEGFR signals with respect to total EGFR was quantified by densitometry analysis. Actin was used as a loading control.
(**G**) Total lysates of scr-CTR and CIP4-KD MCF10A cells treated or not with acute EGF for 5 minutes were immunoblotted for indicated protein. The anti-pY-N-WASP detects tyrosine 256 phosphorylation, which occurs when N-WASP is in an open and actin conformation.

Figure S4: Fibronectin, but not vitronectin or laminin adhesion rescue impaired myosin light chain phopshorylation and scattering. (Related to Fig. 2A and 3C).
(**A-B**) EGF-deprived scr-CTR and CIP4-KD #1 MCF10A cells plated either on gelatin (A) or Fn (B) were stimulated with EGF and stained with the anti-pMLC antibodies or phalloidin to detect F-actin (see also Fig. 3A and E). Bar, 25 μm.
(**C**). scr-CTR and CIP4-KD #1 MCF10A cells were grown in complete media either on plastic (uncoated) or on FN. Phase contrast images are shown. Bar, 100 μm.

(**D**) EGF-deprived scr-CTR and CIP4-KD #1 MCF10A cells plated on plastic, or fibronectin (Fn), or on laminin (Lm) or vitronectin (Vn) were stimulated with EGF and monitored by time lapse. Cell scattering was quantified as described in Fig. 2D by tracking individual cells, measuring the accumulated distance covered by cells from the original position at time 0 within a cell cluster. Example of tracks covered by individual cells for the entire time of the scattering experiments is shown on the left. The % of control of accumulated scattering distance of at least 20 cells/experiments (n = 3 independent experiments) is plotted on the right. (**P<0.05; ***P*<0.01 compared to scr-CTR MCF10A cells). (see also representative Movie S6)

Figure S5: CIP4 loss has a marginal impact on integrin-mediated adhesion, β1 integrin levels and signaling, despite a slight reduction of β1 integrin internalization. (Related to Fig. 3A-B)

(A) The attachment of MCF10A cells to poly-D-lysin (PDL), fibronectin (Fn), laminin (Ln) or Vitronectin (Vn) was monitored using the xCELLigence system as described in Material and Methods.

(**B**) Representative phase contrast images from MCF10A cells growing on fibronectin (10 μg/ml) from which the cell area was measured. Bar is 25 μm. Right graph quantification of the average spreading area.

(**C**) Growing scr-CTR and CIP4-KD #1 MCF10A cells were detached and plated either on Poly-D-Lysin (PDL) or on fibronectin (Fn). At the indicated times, cells were lysate and immublotted with the indicated antibodies.

(**D**) Flow cytometric analysis of cell surface α5β1 and β1 integrins in growing scr-CTR and CIP4-KD MCF10A cells.

(E) Internalization of total and active β1 integrin was monitored in scr-CTR and CIP4-KD #1 MCF10A cells in absence and presence of EGF (100 ng/ml). Mean values ± SD; p< 0.001.

Figure S6: EGF-induced internalization of E-cadherin is reduced by loss of CIP4 and SRC pharmacological inhibition. (Related to Fig. 4).

(**A**) Internalization of E-cadherin was assessed in scr-CTR and CIP4-KD #1 MCF10A cells following EGF-stimulation, at the indicated time points, using an anti-E-cadherin antibody that recognizes the extracellular domain (HECD-1), as described in Suppl. Experimental Procedure. Total surface-bound E-cadherin in untreated controls that were not subjected to acid wash is also shown (0 NW). Internalized E-cadherin was quantified by measuring the intensity of the signal over the number of cells and the area of the field in μm^2. The quantification and selected time points are shown in Fig. 4E. Bar, 15 μm.

(**B**) Efficacy of SRC inhibitors PP2 (10 μM) and Dasatinib (100 nM) was evaluated by immunoprecipitating SRC from lysates of control (scr-CTR) and CIP4-KD MCF10A cells, treated as shown, and IB with the indicated antibodies.

(**C**) EGF-induced E-cadherin internalization was monitored in scr-CTR and CIP4-KD #1 MCF10A cells, treated with DMSO as control or PP2 (10 μM) or dasatinib (100nM), using the anti-E-cadherin HECD-1 antibody as described in Fig. 4E.

(**D**) EGF-induced cell scattering of scr-CTR and CIP4-KD MCF10A cells treated with DMSO as control or PP2 (10 μM) or dasatinib (100nM). Cell scattering was quantified by tracking individual cells, measuring the accumulated distance covered by cells from the original position at time 0 within a cell cluster. The % of control of accumulated scattering distance of at least 40 cells/experiments (n = 3 independent

experiments) is plotted on the right. (***P<0.005 compared to scr-CTR MCF10A cells) (see representative Movie 7).

Figure S7: Clinical features of TMA and CIP4 antibody characterization. (Related to Fig. 7)
(**A**) The clinical and pathological information of the patients included in the case-control TMA operated at the European Institute of Oncology (IEO) between 1994 and 1997 is reported. Disease recurrence (any event and distant relapse) was within 18 years (median 9.2 years and 10.6 years respectively). For some patients not all information was available. Nottingham Prognostic Index (NPI) combines nodal status, tumor size and histological grade. According to NPI's score patients can be divided into 3 classes: Good Prognosis Group (GPG), Moderate Prognosis Group (MPG) and Poor Prognosis Group (PPG).
(**B**) Specificity of the anti-CIP4 antibodies used for the IHC analysis of human tumors. Control and CIP4-KD #1 MCF10A, HeLa and MDA-MB-231 cells were embedded in paraffin and stained with anti-CIP4 antibody.

Figure S8: CIP4 is required for invasion of ERBB2-dependent breast cancer cell. (Related to Fig. 8)
(**A**) Invasion of 10A.ERBB2 scr-CTR and CIP4-KD cells was assessed during 48 hours using ethanol as a control and AP1510 (100 nM) or EGF (100 ng/ml) as chemoattractant. Representative images are shown and invasion was quantified as described in Material and methods. Data are the mean± s.e.m. *p<O.01 and ***p<0.005, as compared to scr-CTR 10A.ERBB2 cells (n=3 independent experiments). Bar is 200 μm.
(**B**) Total cell lysates from various human breast cancer cell lines were immunoblotted with the indicated abs. Please note that CIP4 levels are particularly elevated in the ERBB2+ HCC-1954 line. Triple negative (ER-, PgR-and ERBB2-) and ERBB2+ breast cell lines are indicated.
(**C-D**) HCC-1954 cells were stably transfected with lentiviral vectors encoding for scrambled shRNA (scr-CTR) and CIP4-shRNA (CIP4-KD #2), as described previously, and blotted for CIP4 and vinculin as loading control. Equal number of scr-CTR and CIP4-KD HCC-1954 were seeded sparsely. Representative phase contrast images are shown.
(**E**) Invasion of scr-CTR and CIP4-KD HCC-1954 cells was assessed during 48 hours using vehicle as a control and a mixture of EGF (100 ng/ml) or HGF (20 ng/ml) as chemoattractant. Representative images are shown on the left and invasion was quantified as described in Material and methods. Data are expressed as the % of invasion of scr-CTR cells invading toward the chemotactic mixture and are the mean± s.e.m. *p<0.01 and ***p<0.005, as compared to scr-CTR HCC-1954 cells (n=3 independent experiments). Bar is 100 μm.

Supplemental Movie legends
Movie S1: Random migration of MCF10A cells silenced for TOCA family members. Related to Fig. S2A-B. Random migration of scr-CTR, CIP4-KD#1, TOCA-1-KD, FBP17-KD, 2KD and 3KD MCF10A cells was monitored in complete medium over a 24-hour period with pictures taken every 15 minutes.

Movie S2: EGF-induced cell scattering is delayed in CIP4-KD MCF10A cells. Related to Fig. 1G-H.
scr-CTR and CIP4-KD#1 MCF10A cells were EGF-starved for 24 hours before the addition of 100 ng/ml EGF. Cell scattering was then monitored over a 24-hour period with pictures taken every 5 minutes.

Movie S3: Dynamics of E-cadherin-GFP in MCF10A cells upon EGF stimulation. Related to Fig. 2 and Fig. 4B.
Scr-CTR and CIP4-KD #1-MCF10A cells were transfected with E-cadherin-GFP and EGF-starved for 24 hours. Internalization of E-cadherin was monitored after EGF addition (100 ng/ml) over a 4-hour period with pictures taken every 2 minutes.

Movie S4. **CIP4 loss impairs EGF-induced decreases of FRET efficiency of EcadTSMod at cell–cell junctions. Related to Fig. 2C.**
EGF-starved Scr-CTR and CIP4-KD#1 MCF10A cells were microinjected with the EcadTSMod-CFP(E2) construct or EcadTSModΔcyto-CFP(E2) (not shown) before the addition of 100 ng/ml EGF. Cell scattering was monitored by fluorescence timelapse microscopy over a 5 h period. Pictures were taken every 10 minutes. CFP and the derived FRET/Ratio channels on cell-cell junction, delimited by defining manually the appropriate Region of Interest, are shown. Bar, 10 μm.

Movie S5: EGF-induced scattering of control and CIP4-KD MCF10A cells on different ECM. Related to Fig. 2A and S4D.
*-Left Movies, EGF-induced cell scattering of CIP4-KD MCF10A cells is rescued by plating cell onto fibronectin***.** Scr-CTR and CIP4-KD #1 MCF10A cells were plated on tissues culture plastic dish that were either left untreated or coated with 10 μg/ml of FN. Cells were EGF-starved for 24 hours before the addition of 100 ng/ml EGF. Cell scattering was then monitored over a 24-hour period with pictures taken every 5 minutes.
Related to Fig. 2A.
*-Right Movies, EGF-induced cell scattering of CIP4-KD MCF10A cells is rescued by plating cell onto fibronectin, but not on Laminin or Vitronectin***.** Scr-CTR and CIP4-KD #1 MCF10A cells were plated on tissues culture plastic dish that were either left untreated (plastic) or coated with 10 μg/ml of fibronectin, or Laminin (LM) or vitronectin. Cells were EGF-starved for 24 hours before the addition of 100 ng/ml EGF. Cell scattering was then monitored over a 24-hour period with pictures taken every 15 minutes.
Related to Fig. S4D.

Movie S6: Effects of SRC inhibition and of CIP4 mutant no longer binding to SRC on EGF-induced scattering of MCF10A. Related to Fig. S6B and 5F.
*-A, Left Movies***,** *EGF-induced cell scattering of CIP4-KD MCF10A cells is impaired by pharmacological inhibition of SRC***.** Scr-CTR and CIP4-KD #1 MCF10A cells were plated on tissues culture plastic dish. Cells were EGF-starved for 24 hours before the addition of 100 ng/ml EGF in the presence of DMSO, as vehicle, or 100 μM of PP2 or 100 nM of Dasatinib. Cell scattering was then monitored over a 24-hour period with pictures taken every 15 minutes.
Related to Fig. S6B
-B, Right Movies: EGF-induced cell scattering of CIP4-KD MCF10A cells is rescued by the expression of a siRNA resistant wild type CIP4, but not an SRC-binding

defective ΔP-CIP4 mutant. scr-CTR and CIP4-KD #1 MCF10A were lentivirally infected with either an empty vector or with vector expressing siRNA-resistant WT- (resCIP4-WT) or ΔP-CIP4 (resCIP4-ΔP) mutants. Cells were EGF-starved, before stimulation with 100 ng/ml EGF. Cell scattering was monitored by time-lapse video microscopy over a 24-hour period with pictures taken every 15 minutes.
Related to Fig. 5F

Supplemental Experimental Procedures

Antibodies and reagents

Mouse monoclonal anti-TOCA-1 was raised against amino acids 416–470 fused to GST. Polyclonal anti-EGFR is against amino acids 1172-1186. The rabbit serum anti-FBP17 (YU520) was kindly provided by Dr. Pietro De Camilli (Yale University School of Medicine, Connecticut, USA). Polyclonal anti-human CIP4 serum was kindly provided by Dr. Andrew Craig (Queen's University, Ontario, Canada). Monoclonal antibodies directed against actin and vinculin were from Sigma. Antibodies directed against phospho-EGFR (Tyr1068), AKT, phospho-AKT (Ser473), ERK1/2, phospho-ERK1/2 (p42-44), phospho-SRC Family (Tyr416), phospho-Smad3 (C25A9) and Smad3 (C67h9), polyclonal anti-phospho-Myosin Light Chain 2 (Thr18/Ser19) antibodies were from Cell Signaling. Anti-CIP4, -N-cadherin and -E-cadherin were from BD transduction Laboratories. Monoclonal HECD-1 anti-E-cadherin, anti-giantin, Anti-β1-integrin (total-ab30388), Anti-N-WASP (phospho Y256) antibody ab23395 were from Abcam. Anti-SRC (clone GD11) was from Millipore and mouse anti-integrin a5β1 monoclonal antibody (P1D6) was from Immunological Sciences. Anti-active-β1-integrin was from BD Pharmingen (9EG7, 550531). Mouse anti-integrin β1 (K-20) was from Santa Cruz Biotechnology. Secondary antibodies conjugated to: horseradish peroxidase were from Bio-Rad; Cy3 were from Amersham; Alexa Fluor® 488 were from Molecular Probes. TRITC- and FITC-conjugated phalloidin were from Sigma Aldrich. EZ-Link^{TM} Sulfo-NHS-SS-Biotin was from Thermo Scientific. MESNA and Streptavidin-Agarose beads were from Sigma, while Nitrocellulose transfer membrane was from Whatman. SRC inhibitor PP2 (4-amino-5-(4-chlorophenyl)-7-(t-butyl) pyrazolo[3,4-d]pyrimidine) was from Gibco. E-cadherinTsMod_CFP(E2): The E-cadherinTSMod-CFP(E2) construct was generated by modification of the previously published E-cadherinTsMod construct (Borghi et al., 2012). The original E-cadherinTsMod was assembled (Epoch Life Science) from canine E-cadherin cDNA (Adams et al., 1998) and the TSMod sequence (Grashoff et al., 2010). In the TsMod of E2 construct mTFP was substituted for CFP. Resulting modified TsMod bearing CFP and EYFP (Venus) separated by flexible flagella sequence, was flanked with linkers A: GGATCAGGTGGAACTGGTTCAACATCTGGAGGTTCAGGAGGTTCAACAGG AGGTGGAACAGGAGG upstream and B**:**GGATCAGGTGGAACTGGTTCAACATCTGGAGGTTCAGGAGGTTCAACA GGAGGT downstream and inserted between V742 and K743 of E-cadherin, which are the fourth and fifth residues of the juxtamembrane domain, respectively.

The above modifications, CFP swap and longer linkers, enable the resulting fusion protein to be less prone to aggregation. E-cadherin TsoModΔCyto_CFP: The EcadTSModΔcyto-CFP construct assembled from E-cadherin residues 1–758 appended with the TSMod sequence bearing CFP fused through the linker A. E-cadherin TsMod-CFP(E2) only was used to control for bleed through estimation was assembled by deletion of the EYFP(Venus) from E-cadherinTsMod-CFP(E2).

Immunohistochemistry and TMA analysis

Immunohistochemical analyses of CIP4 expression were performed on formalin-fixed paraffin-embedded breast TMA tumor sections obtained from tumor breast biopsies using a commercial Rabbit monoclonal antibody (Abcam, AB108313, clone EPR1965), which was used at a dilution of 1:1,500 following an antigen retrieval

procedure in EDTA pH 8.0. Immunocomplexes were visualized by the EnVision™+ HRP. Rabbit (DAB+), DAKO (K4011), and acquired with the Aperio ScanScope system. CIP4 expression was measured in parallel in a group of normal breast samples (N=38). In normal tissue CIP4 is expressed at low level (median score =0.5, mean score =0.68). CIP4 high expression was defined when tumors display an expression score >1. Tumors were consequently divided in CIP4-high and CIP4-low according to the score assigned.

Cell culture and transfection

The immortalized human mammary epithelial cell line MCF10A.ErbB2 (kindly provided by Muthuswamy, S.K.) and MCF10A were cultured in DMEM/F12 medium supplemented with 5% donor horse serum, 20 ng/ml EGF, 10 µg/ml insulin, 0.5 µg/ml hydrocortisone and 100 ng/ml cholera toxin at 37°C in a humidified atmosphere with 5% CO_2. MCF10A cells were transduced with pLKO.1-scr-CTR (scrambled control sequence), pLKO.1-shCIP4#2, pLKO.1-shTOCA-1, pLL3.7-shCIP4#1, and pLL3.7-shFBP17 lentiviruses, and selected with the appropriate antibiotic to generate the scr-CTR, CIP4-KD #2, TOCA-1-KD, CIP4-KD #1 and FBP17-KD cells, respectively. CIP4-KD #1 MCF10A cells were also subjected to a second round of infection with the pLKO.1-shTOCA lentivirus (designated 2KD), and a third round of infection with the pLL3.7-shFBP17 lentivirus (designated 3KD). Where specified, cells were EGF- and serum-starved for 18 hours and treated with 5 ng/ml TGF-β1 (R&D Systems, Inc.) or vehicle (4 mM HCl, 1 mg/ml BSA) for different time points. When PP2 was used, cells were treated for 18 hours with 10 µM PP2 or DMSO control in medium without EGF.

For rescue experiments, cells were transfected with peGFP empty vector or resistant-CIP4-peGFP plamid (res-CIP4-peGFP) using Amaxa® Nucleofector® kit V formulated by Lonza. Briefly, cells ($1x10^6$) were transfected with 5 µg of appropriate plasmid using program T-024 of the Nucleofector® I Device and lysed for protein analysis. For immunofluorescence and epifluorescence analysis, transfected cells were seeded on glass coverslips and fixed 24 hours after transfection.

Generation of lentiviruses particles

Lentiviruses were produced by co-transfection of HEK293T cells with a pLKO.1-based plasmid or pLentiLox 3.7 (pLL3.7) and packaging vectors (pCMVΔR8.91, VSV-G, Rev, pMDL) via the calcium phosphate method. Two batches of conditioned medium were collected after 48 and 72 hours and filtered through 0.45 µm filters. MCF10A cells were transduced with viral supernatants and cell pools were selected using puromycin (1 µg/ml), hygromycin (100 µg/ml) and/or neomycin (150 µg/ml). After several passages, cell pools were selected based on the efficiency of shRNA by protein analysis (shCIP4 target sequence#1: 5'-GGAGGTGGTGCCCATAATA-3', #2 and 5′-GCAACAGTCCTTCGTACAGAT-3; shTOCA1 target sequence: 5'-CGCACAGAGTGTATGGTG-3', shFBP17 target sequence: 5'- GATCAGTTTGAC AACTTA-3').

Immunoprecipitation and immunoblotting

Cells were lysed in lysis buffer (50 mM Tris-HCl pH8.0, 150 mM NaCl, 5 mM EGTA, 1.5 mM $MgCl_2$, 10% glycerol, 1% Triton X-100, 1 mM Na_3VO_4, 10 µg/ml aprotinin, 10 µg/ml leupeptin) and centrifuged at 16,100*g* for 30 minutes at 4°C. Soluble cell lysates were subjected to immunoprecipitation with anti-E-cadherin, anti-SRC or anti-CIP4 antibodies. Antibody-protein complexes were recovered with

protein G-Sepharose (GE Healthcare). Proteins were then separated by SDS-PAGE, transferred onto a Protran® nitrocellulose membrane and probed with the appropriate antibodies.

Quantitative RT-PCR detection of mRNAs

Total RNA was extracted from MCF10A cells using the Trizol reagent (Invitrogen). Reverse transcription was performed using SuperScript® VILO™ cDNA Synthesis Kit (Invitrogen). Gene expression was measured using TaqMan Gene Expression Assays (Applied Biosystems). 18S was used as an internal control to normalize mRNA levels. Real-time PCR quantitation of transcripts was expressed as fold increase with respect to 90 minutes treatment with vehicle for respective MCF10A cell sublines.

Immunofluorescence

MCF10A cells ($1x10^5$) were seeded in a 100 mm diameter dish containing glass coverslips and grown in complete medium for 3 days. Where applicable, cells were EGF-starved for 24 hours prior to staining. Cells were then washed with PBS, fixed with 4% paraformaldehyde and permeabilized with 0.5% Triton X-100. After blocking with 3% BSA, primary antibodies were added for 1 hour at room temperature. Cover slips were washed in wash solution (130 mM NaCl, 0.1% BSA, 0.2% Triton X-100, 0.05% Tween 20, 15 mM PBS pH 7.4) before incubation with Alexa-Fluor-488- or CY3-conjugated IgG at room temperature for 1 hour. TRITC- or FITC-conjugated phalloidin was added in the secondary antibody mixture. After washing, coverslips were incubated with 0.5 ng/ml DAPI, post-fixed and mounted on slides. Images were taken with a *Leica* TCS *SP2* confocal microscope.

Extended version of the ^{125}I-EGF internalization and recycling assays.

EGFR surface levels and EGF Internalization and recycling assays with ^{125}I-EGF were performed as described in (Sorkin and Carpenter, 1991; Sorkin and Duex, 2010; Sorkin et al., 1991).

*EGFR surface levels***:** Serum and EGF-starved MCF10A cells were incubated on ice for 7 hours in the presence of 100 ng/ml EGF (20 ng/ml ^{125}I-EGF plus 80 ng/ml cold EGF) in DMEM/F12 medium supplemented with 2% BSA. Cells were washed 3 times with ice-cold PBS and solubilized in 1 M NaOH. After correction for the hot/cold dilution, the number of receptors on the surface was deduced from the specific activities of the labeled ligand. Non-specific binding was measured for each time point in the presence of a 100-200–fold excess of cold ligand, and was never > 3-10 % of the total counts

*Internalization assay***:** MCF10A cells were EGF-starved for 18 hours before the addition of 2 ng/ml ^{125}I-EGF in the binding medium (DMEM/F12 medium containing 20 mM Hepes and 0.1% BSA) for 2, 4 and 6 minutes at 37°C. Afterwards, cells were transferred on ice, washed with cold PBS pH 7.4 and incubated for 5 minutes in acid wash buffer (0.5 M NaCl, 0.5 M acid acetic). This soluble fraction represents the amount of ^{125}I-EGF bound to the receptor on the cell surface. Cells were then dried at room temperature for 5 minutes and lysed with 1 N NaOH. This lysate represents the amount of internalized ^{125}I-EGF. The rate of internalization is expressed as the ratio between internalized and surface ^{125}I-EGF for each time point. A low concentration of ^{125}I-EGF was used to avoid saturation of the internalization machinery. Specific binding is reported for all data points. Non-specific binding was measured by adding a 200-fold excess of cold EGF.

Recycling assay: ^{125}I-EGF recycling assays were performed exactly as described (Sorkin and Carpenter, 1991). Briefly, cells were EGF-starved and then incubated with ^{125}I-EGF (20 ng/ml) for 15 minutes at 37°C, followed by mild acid/salt treatment (0.2 M Na acetate pH 4.5, 0.5 M NaCl) to remove bound EGF. Cells were then chased at 37°C in medium containing 4 μg/ml EGF for the indicated times, to allow recycling. At the end of each chase time, the medium was collected and subjected to TCA precipitation to determine the amount of intact (TCA precipitable) and degraded (TCA soluble) ^{125}I-EGF present. Surface-bound ^{125}I-EGF was extracted by acid treatment (0.2 M acetic acid pH 2.8, 0.5 M NaCl). Finally, cells were lysed in 1N NaOH to determine intracellular ^{125}I-EGF. Data are expressed as the percentage of intact internalized ^{125}I-EGF in the medium with respect to the total ^{125}I-EGF (total medium + total surface + total intracellular). Non-specific counts were measured for each time point in the presence of a 200-fold excess of cold ligand, and were never > 3-10% of the total counts.

Extended version of the total and active β1 integrin internalization.

Internalization of total and active β1 integrin was assessed as in (Roberts et al., 2001). Briefly, ice-cold cells were surface-labeled at 4 °C with 0.5 mg/ml sulfo-NHS-SS-biotin (ThermoScientific) in cold PBS for 30 min. After washing the cell extensively, they were transferred to prewarmed DMEM 1% FBS at 37 °C containing 0.2 mM primaquine, to inhibits recycling from endosomes (van Weert et al., 2000). At the indicated times, biotin was removed from proteins remaining at the cell surface by incubation with a solution containing 20 mM sodium 2-mercaptoethanesulfonate (MesNa) in 50 mM Tris-HCl (pH 8.6), 100 mM NaCl, 0.015 N NaOH for 1 h at 4°C. MesNa was quenched by the addition of 20 mM iodoacetamide for 10 min. Cells were washed in PBS then lysed in 25 mM Tris-HCl, pH 7.6, 100 mM NaCl, 2 mM MgCl2, 1 mM Na3VO4, 0.5 mM EGTA, 1% Triton X-100, 5% glycerol, protease mix (Sigma), and 1 mM PMSF. Equal amount of total cellular lysates were used in capture-ELISA assays as in (Roberts et al., 2001) using mouse anti-β1 integrin (Abcam ab30388) or rat anti-active-β1 integrin 9EG7 (BD Pharmingen 550531).

References

Adams, C.L., Chen, Y.T., Smith, S.J., and Nelson, W.J. (1998). Mechanisms of epithelial cell-cell adhesion and cell compaction revealed by high-resolution tracking of E-cadherin-green fluorescent protein. J Cell Biol *142*, 1105-1119.

Borghi, N., Sorokina, M., Shcherbakova, O.G., Weis, W.I., Pruitt, B.L., Nelson, W.J., and Dunn, A.R. (2012). E-cadherin is under constitutive actomyosin-generated tension that is increased at cell-cell contacts upon externally applied stretch. Proceedings of the National Academy of Sciences of the United States of America *109*, 12568-12573.

Grashoff, C., Hoffman, B.D., Brenner, M.D., Zhou, R., Parsons, M., Yang, M.T., McLean, M.A., Sligar, S.G., Chen, C.S., Ha, T., *et al.* (2010). Measuring mechanical tension across vinculin reveals regulation of focal adhesion dynamics. Nature *466*, 263-266.

Roberts, M., Barry, S., Woods, A., van der Sluijs, P., and Norman, J. (2001). PDGF-regulated rab4-dependent recycling of alphavbeta3 integrin from early endosomes is necessary for cell adhesion and spreading. Curr Biol *11*, 1392-1402.

Sorkin, A., and Carpenter, G. (1991). Dimerization of internalized epidermal growth factor receptors. J Biol Chem *266*, 23453-23460.
Sorkin, A., and Duex, J.E. (2010). Quantitative analysis of endocytosis and turnover of epidermal growth factor (EGF) and EGF receptor. Curr Protoc Cell Biol *Chapter 15*, Unit 15 14.
Sorkin, A., Krolenko, S., Kudrjavtceva, N., Lazebnik, J., Teslenko, L., Soderquist, A.M., and Nikolsky, N. (1991). Recycling of epidermal growth factor-receptor complexes in A431 cells: identification of dual pathways. J Cell Biol *112*, 55-63.
van Weert, A.W., Geuze, H.J., Groothuis, B., and Stoorvogel, W. (2000). Primaquine interferes with membrane recycling from endosomes to the plasma membrane through a direct interaction with endosomes which does not involve neutralisation of endosomal pH nor osmotic swelling of endosomes. European journal of cell biology *79*, 394-399.
Borghi, N., Sorokina, M., Shcherbakova, O.G., Weis, W.I., Pruitt, B.L., Nelson, W.J., and Dunn, A.R. (2012). E-cadherin is under constitutive actomyosin-generated tension that is increased at cell-cell contacts upon externally applied stretch. Proceedings of the National Academy of Sciences of the United States of America *109*, 12568-12573.
Grashoff, C., Hoffman, B.D., Brenner, M.D., Zhou, R., Parsons, M., Yang, M.T., McLean, M.A., Sligar, S.G., Chen, C.S., Ha, T., *et al.* (2010). Measuring mechanical tension across vinculin reveals regulation of focal adhesion dynamics. Nature *466*, 263-266.
Roberts, M., Barry, S., Woods, A., van der Sluijs, P., and Norman, J. (2001). PDGF-regulated rab4-dependent recycling of alphavbeta3 integrin from early endosomes is necessary for cell adhesion and spreading. Curr Biol *11*, 1392-1402.
Sorkin, A., and Carpenter, G. (1991). Dimerization of internalized epidermal growth factor receptors. J Biol Chem *266*, 23453-23460.
Sorkin, A., and Duex, J.E. (2010). Quantitative analysis of endocytosis and turnover of epidermal growth factor (EGF) and EGF receptor. Curr Protoc Cell Biol *Chapter 15*, Unit 15 14.
Sorkin, A., Krolenko, S., Kudrjavtceva, N., Lazebnik, J., Teslenko, L., Soderquist, A.M., and Nikolsky, N. (1991). Recycling of epidermal growth factor-receptor complexes in A431 cells: identification of dual pathways. J Cell Biol *112*, 55-63.
van Weert, A.W., Geuze, H.J., Groothuis, B., and Stoorvogel, W. (2000). Primaquine interferes with membrane recycling from endosomes to the plasma membrane through a direct interaction with endosomes which does not involve neutralisation of endosomal pH nor osmotic swelling of endosomes. European journal of cell biology *79*, 394-399.
Borghi, N., Sorokina, M., Shcherbakova, O.G., Weis, W.I., Pruitt, B.L., Nelson, W.J., and Dunn, A.R. (2012). E-cadherin is under constitutive actomyosin-generated tension that is increased at cell-cell contacts upon externally applied stretch. Proceedings of the National Academy of Sciences of the United States of America *109*, 12568-12573.
Roberts, M., Barry, S., Woods, A., van der Sluijs, P., and Norman, J. (2001). PDGF-regulated rab4-dependent recycling of alphavbeta3 integrin from early endosomes is necessary for cell adhesion and spreading. Curr Biol *11*, 1392-1402.
Sorkin, A., and Carpenter, G. (1991). Dimerization of internalized epidermal growth factor receptors. J Biol Chem *266*, 23453-23460.

Sorkin, A., and Duex, J.E. (2010). Quantitative analysis of endocytosis and turnover of epidermal growth factor (EGF) and EGF receptor. Curr Protoc Cell Biol *Chapter 15*, Unit 15 14.
Sorkin, A., Krolenko, S., Kudrjavtceva, N., Lazebnik, J., Teslenko, L., Soderquist, A.M., and Nikolsky, N. (1991). Recycling of epidermal growth factor-receptor complexes in A431 cells: identification of dual pathways. J Cell Biol *112*, 55-63.
van Weert, A.W., Geuze, H.J., Groothuis, B., and Stoorvogel, W. (2000). Primaquine interferes with membrane recycling from endosomes to the plasma membrane through a direct interaction with endosomes which does not involve neutralisation of endosomal pH nor osmotic swelling of endosomes. European journal of cell biology *79*, 394-399.
Roberts, M., Barry, S., Woods, A., van der Sluijs, P., and Norman, J. (2001). PDGF-regulated rab4-dependent recycling of alphavbeta3 integrin from early endosomes is necessary for cell adhesion and spreading. Curr Biol *11*, 1392-1402.
Sorkin, A., and Carpenter, G. (1991). Dimerization of internalized epidermal growth factor receptors. J Biol Chem *266*, 23453-23460.
Sorkin, A., and Duex, J.E. (2010). Quantitative analysis of endocytosis and turnover of epidermal growth factor (EGF) and EGF receptor. Curr Protoc Cell Biol *Chapter 15*, Unit 15 14.
Sorkin, A., Krolenko, S., Kudrjavtceva, N., Lazebnik, J., Teslenko, L., Soderquist, A.M., and Nikolsky, N. (1991). Recycling of epidermal growth factor-receptor complexes in A431 cells: identification of dual pathways. J Cell Biol *112*, 55-63.
van Weert, A.W., Geuze, H.J., Groothuis, B., and Stoorvogel, W. (2000). Primaquine interferes with membrane recycling from endosomes to the plasma membrane through a direct interaction with endosomes which does not involve neutralisation of endosomal pH nor osmotic swelling of endosomes. European journal of cell biology *79*, 394-399.

Supp. Figure 1

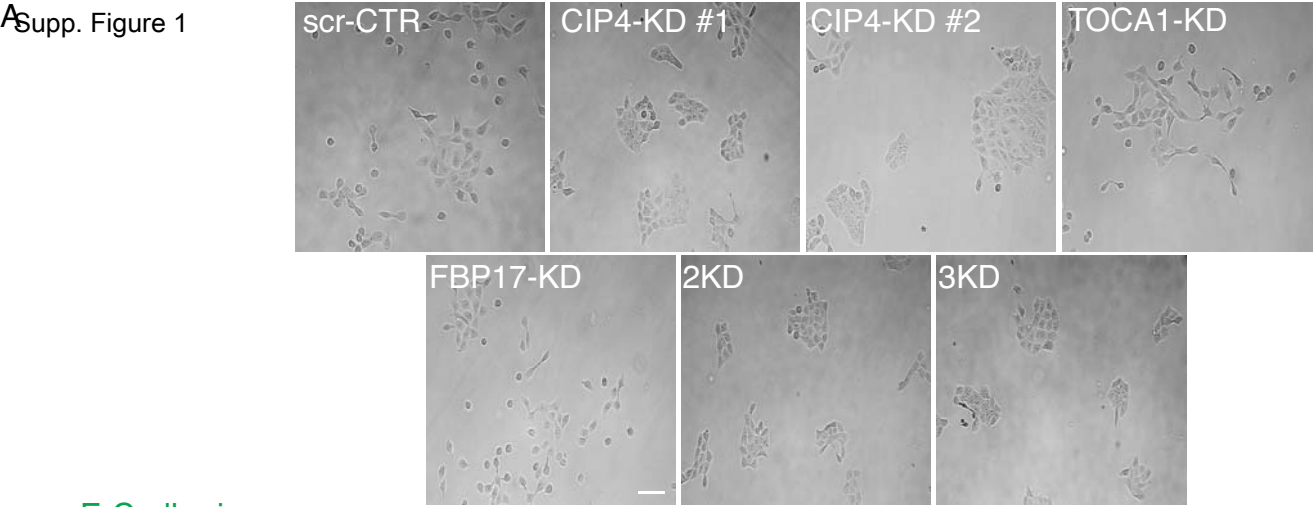

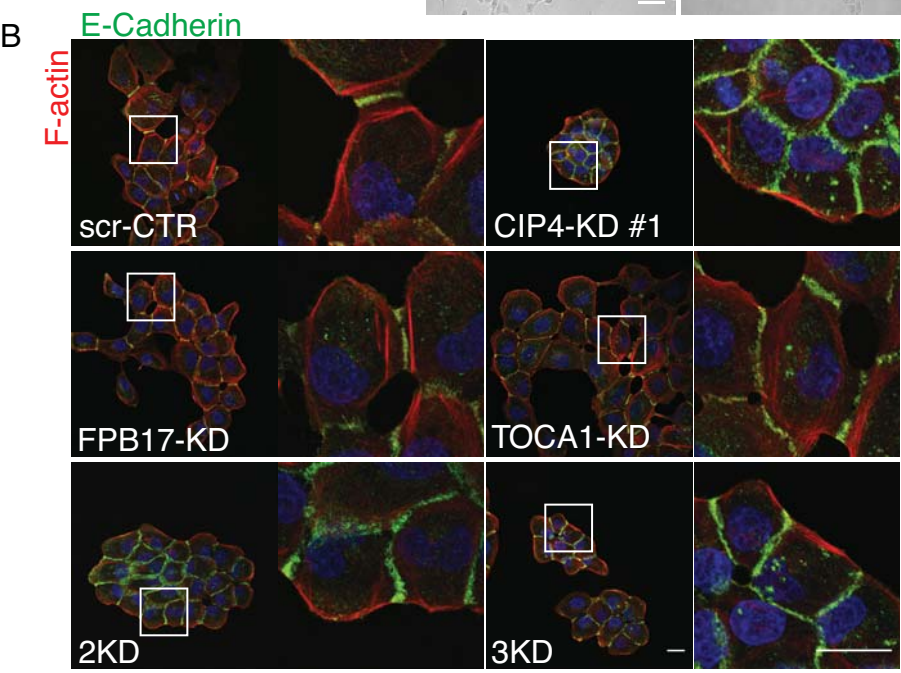

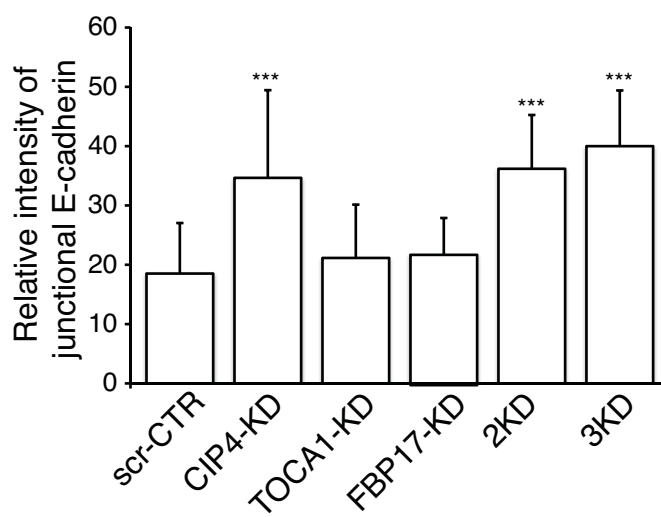

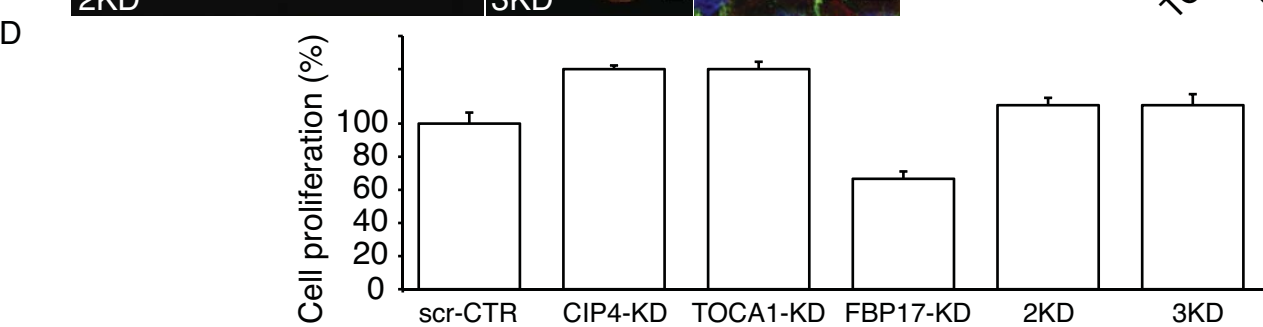

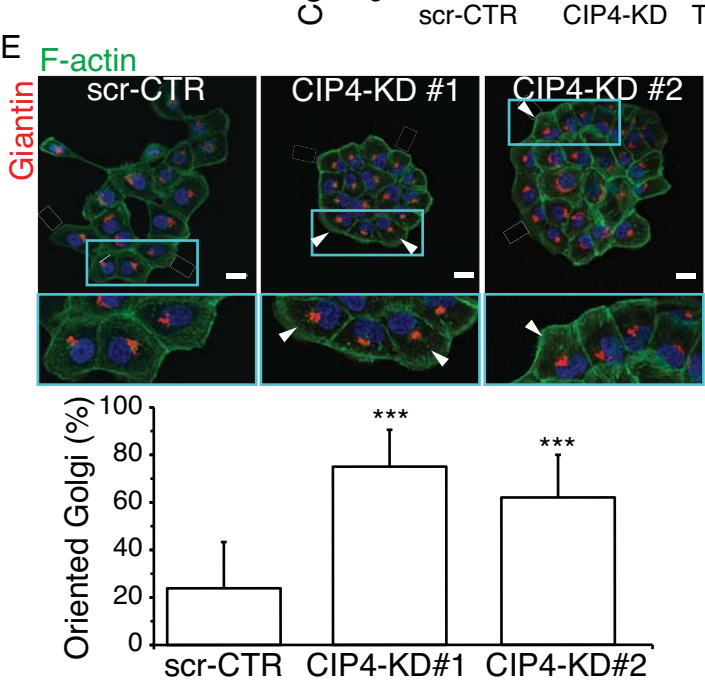

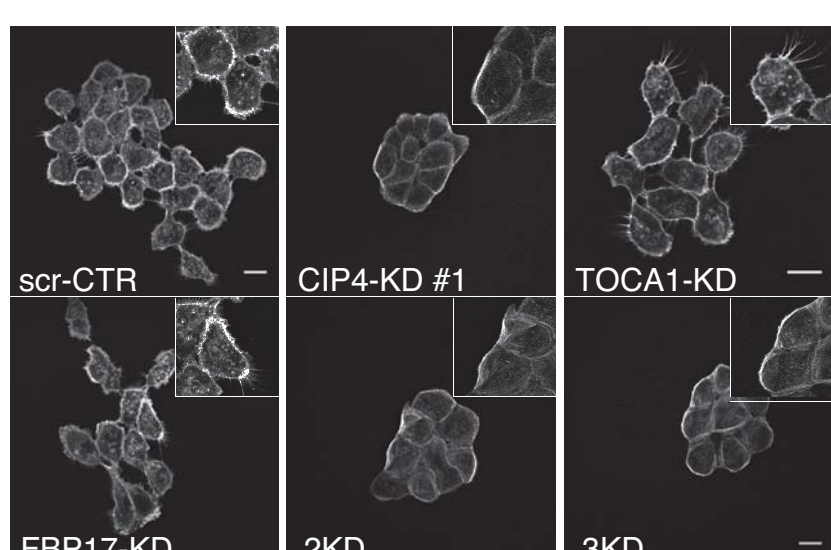

Fig. S1

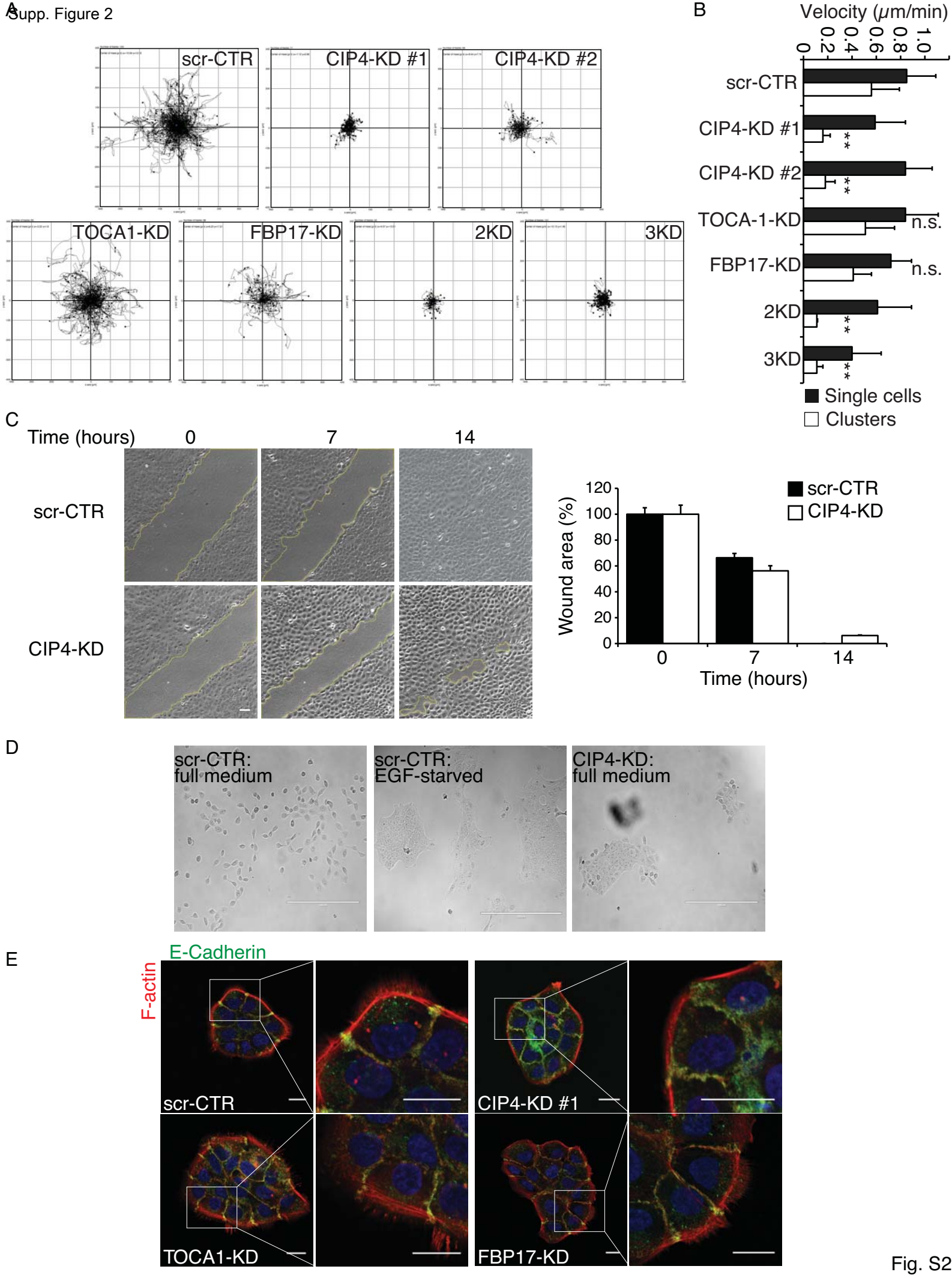
A
scr-CTR
CIP4-KD #1
CIP4-KD #2
TOCA1-KD
FBP17-KD
2KD
3KD
B
Velocity (μm/min)
0
0.2
0.4
0.6
0.8
1.0
scr-CTR
CIP4-KD #1
CIP4-KD #2
TOCA-1-KD
FBP17-KD
2KD
3KD
**
**
n.s.
n.s.
**
**
Single cells
Clusters
C
Time (hours)
0
7
14
scr-CTR
CIP4-KD
Wound area (%)
120
100
80
60
40
20
0
scr-CTR
CIP4-KD
0
7
14
Time (hours)
D
scr-CTR:
full medium
scr-CTR:
EGF-starved
CIP4-KD:
full medium
E
E-Cadherin
F-actin
scr-CTR
CIP4-KD #1
TOCA1-KD
FBP17-KD

Fig. S2

Supp. Figure 3

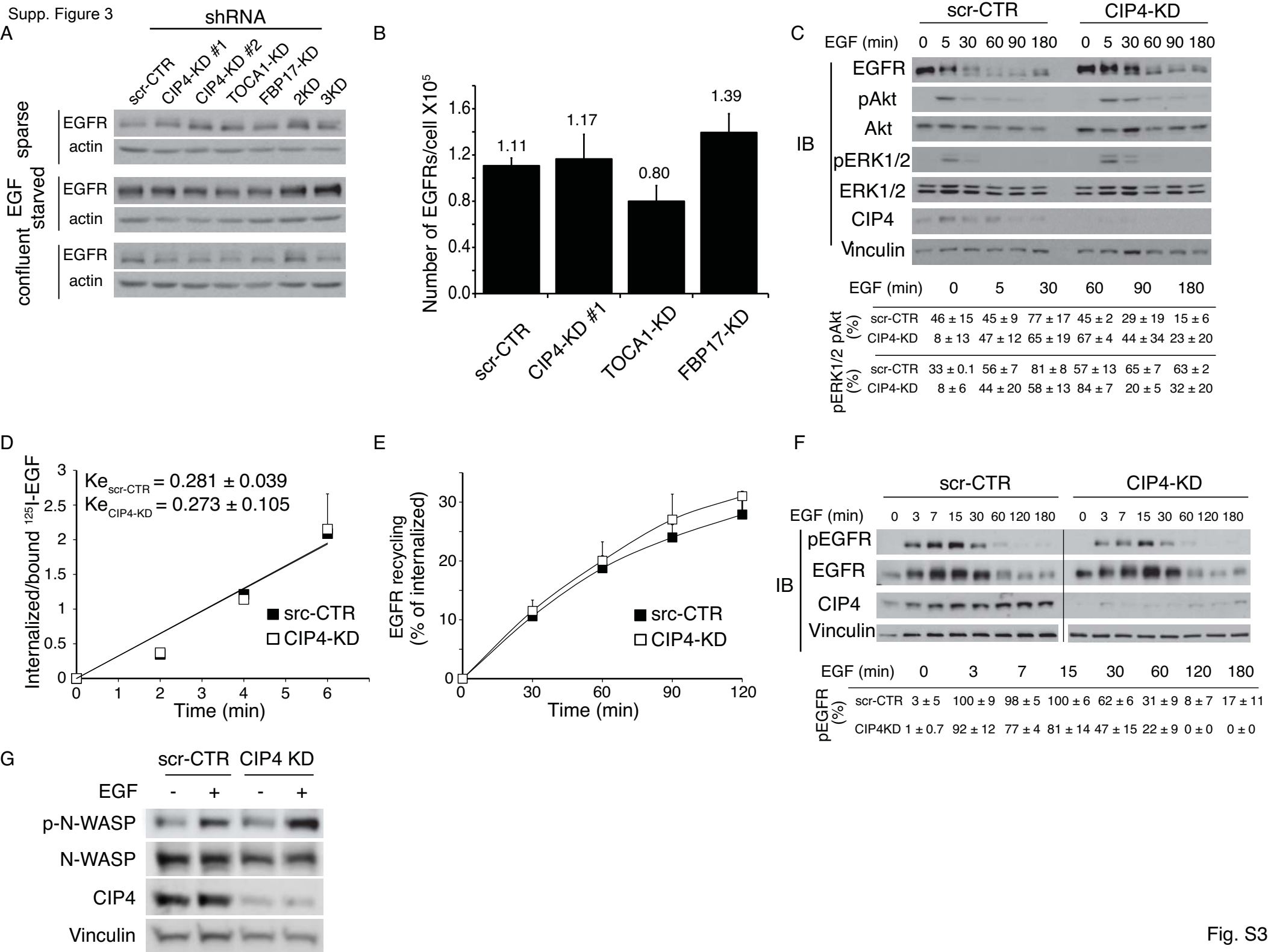

Fig. S3

Supp. Figure 4

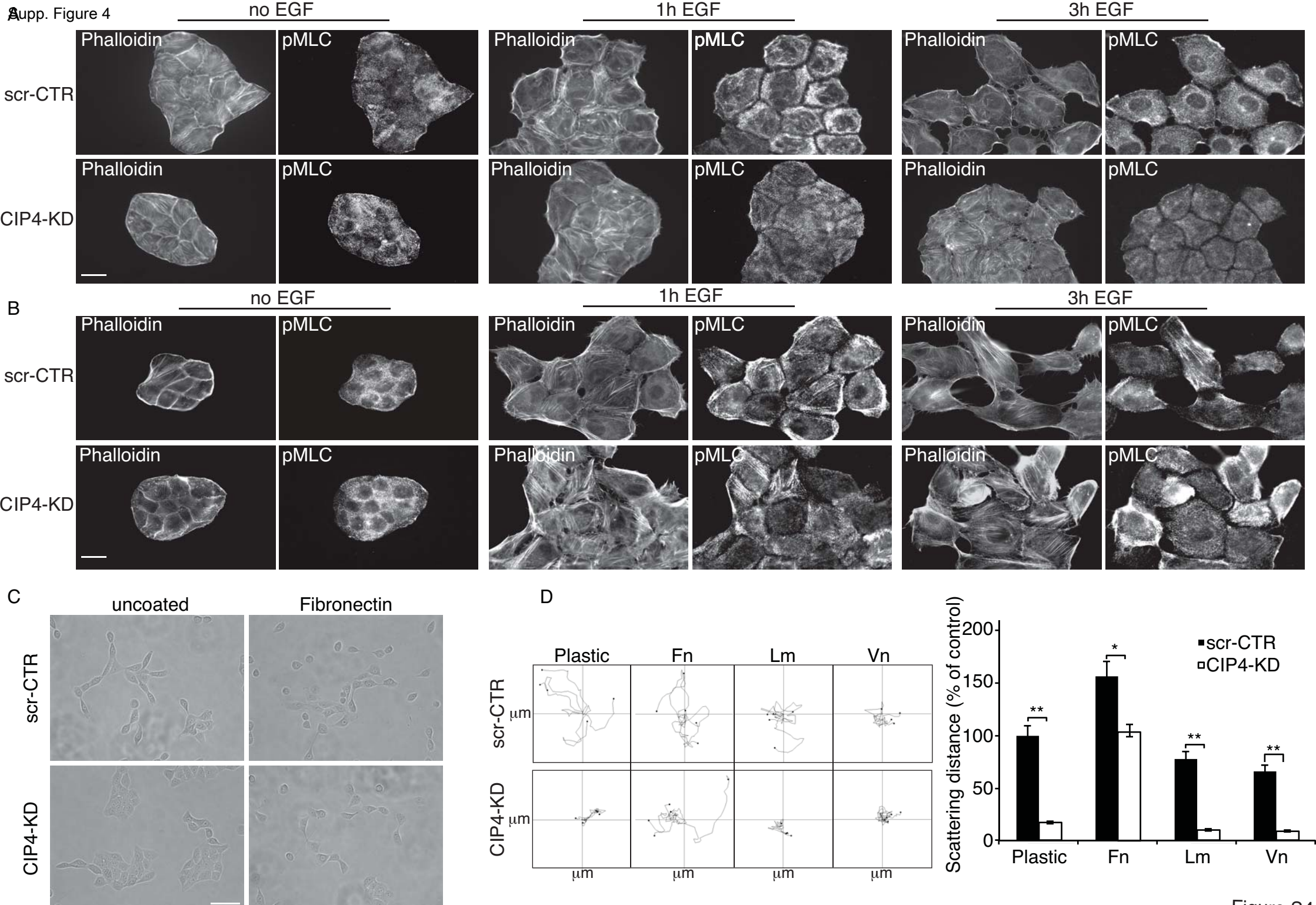

Figure S4

Supp. Figure 5

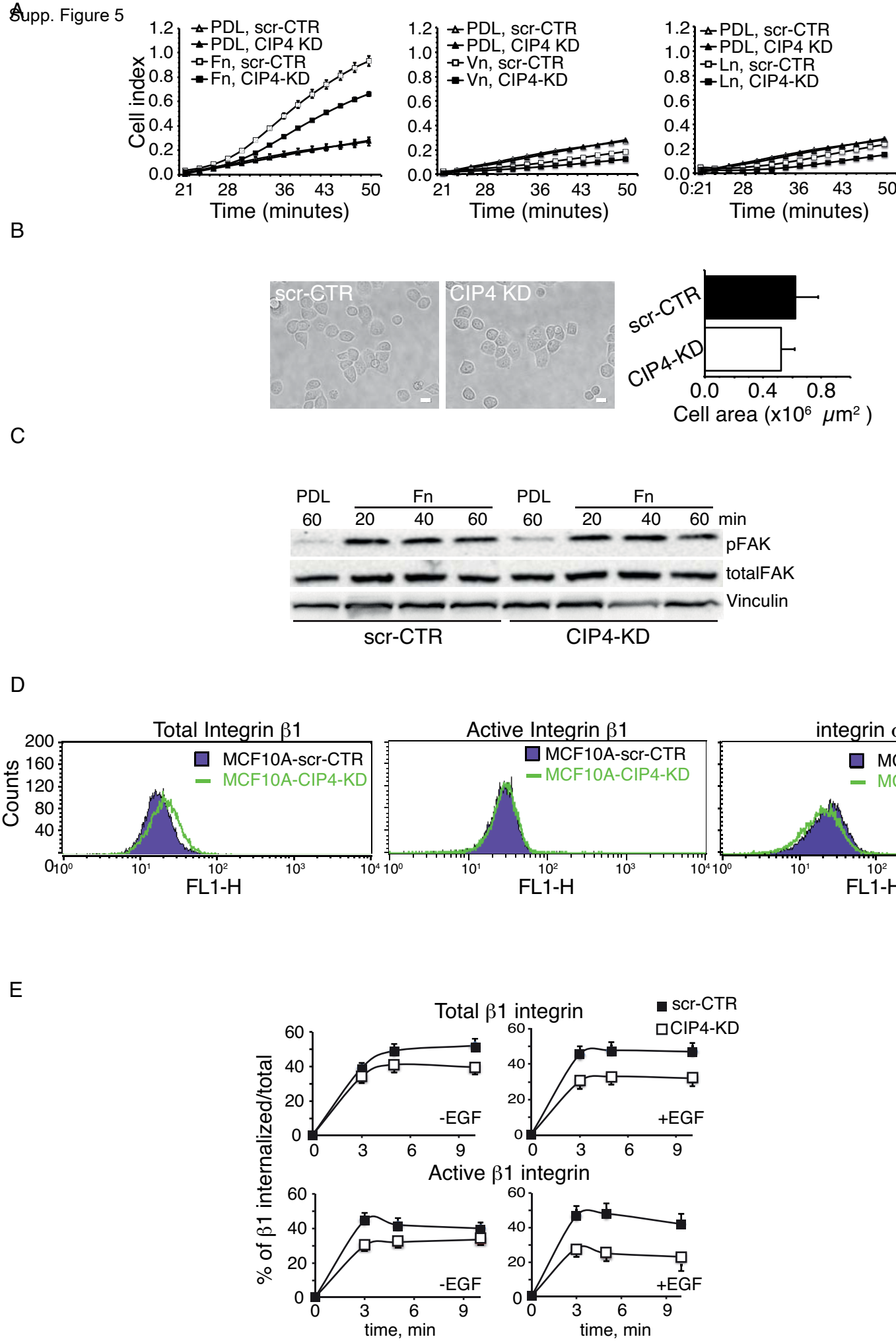

Fig. S5

Supp. Figure 6

A

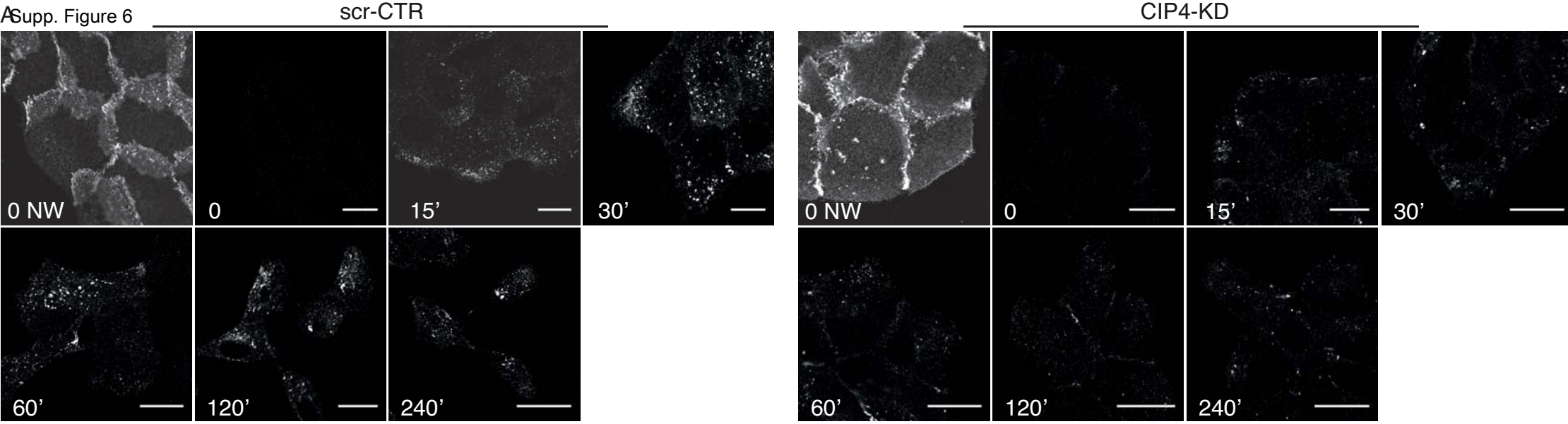

B

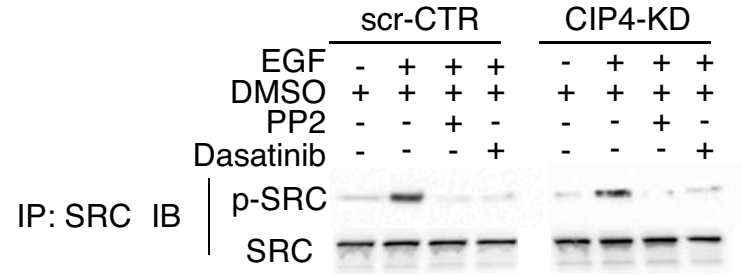

C

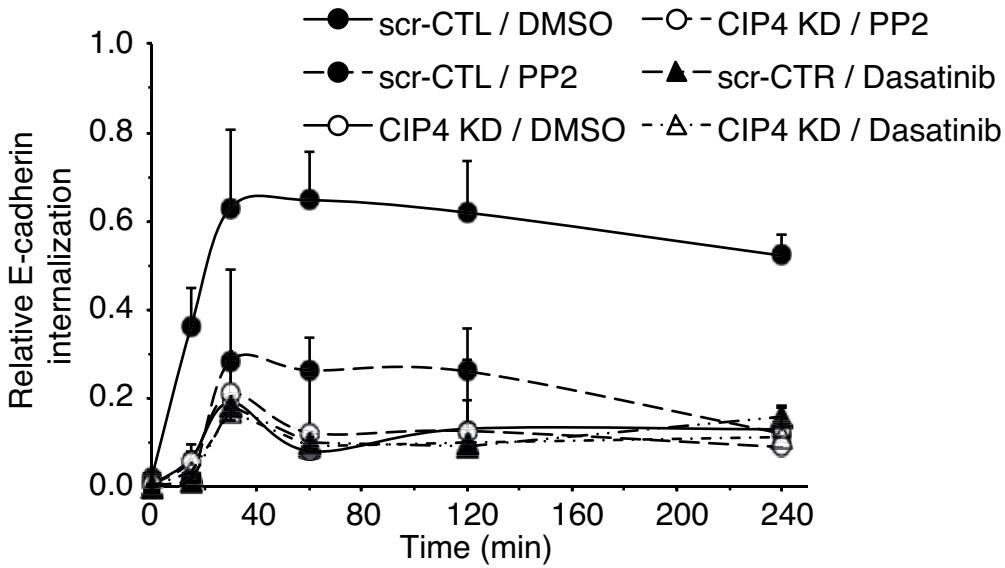

D

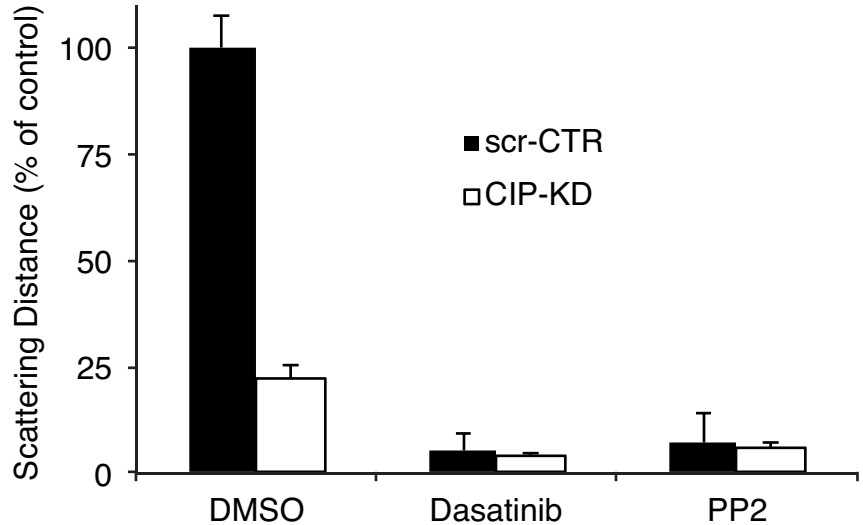

Fig. S6

A Supp. Figure 7

Supplemental Table 1. Clinical and pathological information of the case-control dataset of breast cancer patients

PARAMETER	GROUP	CASE-CONTROL DATASET (N = 349)	
		N	%
Histotype	DUCTAL	290	83.09
	LOBULAR	50	14.33
	OTHER	9	2.58
pT	1	178	51.44
	2	142	41.04
	3	18	5.2
	4	8	2.3
Nodal Status	NEG	153	43.84
	POS	196	56.16
Grade	G1	56	18.42
	G2	132	43.42
	G3	116	38.16
ER	NEG	106	31.45
	POS	231	68.55
PgR	NEG	140	41.54
	POS	197	58.46
Ki-67	NEG	116	34.42
	POS	221	65.58
ErbB2	NEG	227	88.22
	POS	37	11.78
NPI	GPG	84	28
	MPG	133	44.33
	PPG	83	27.67
Any Event	NO	165	47.28
	YES	184	52.72
Distant Relapse	NO	245	70.2
	YES	104	29.8
Status	ALIVE	233	66.76
	DEAD	116	33.24

B

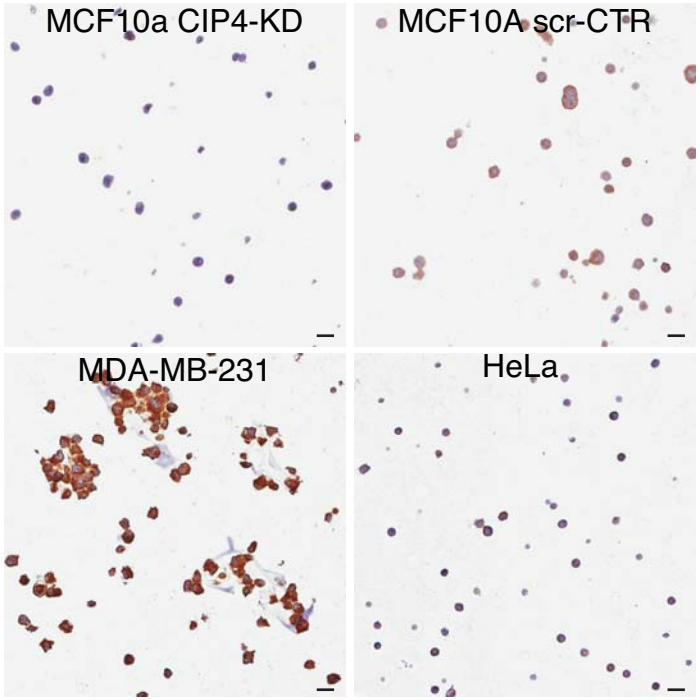

Fig. S7

Supp. Figure 8

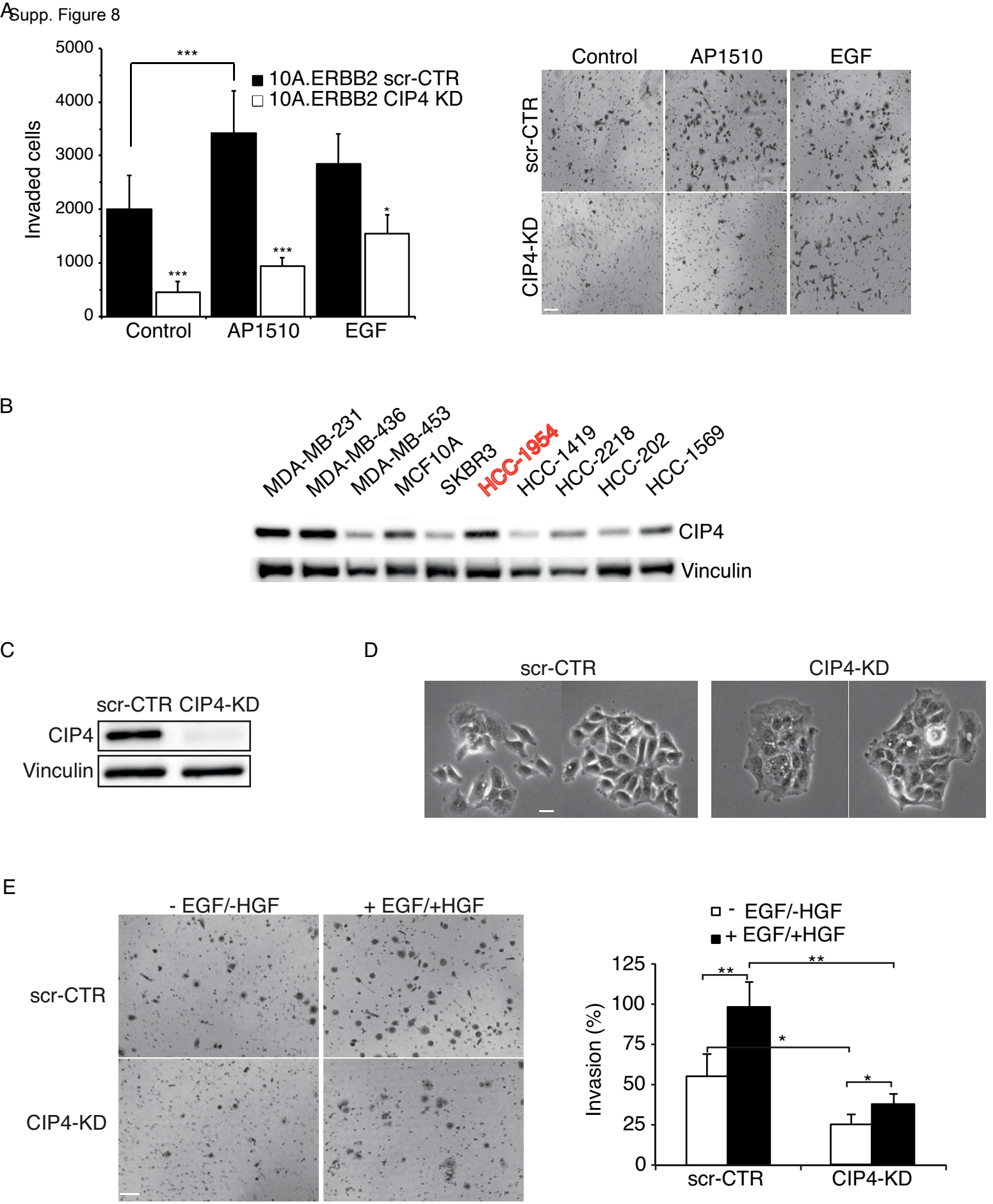

Fig. S8